AD-A033 550 AIR FORCE FLIGHT DYNAMICS LAB WRIGHT-PATTERSON AFB OHIO F/G 1/1
SUBSONIC AND TRANSONIC SIMILARITY RULES FOR JET-FLAPPED WINGS.(U)
OCT 76 H W WOOLARD

UNCLASSIFIED AFFDL-TR-76-86 NL

| OF |
AD A033550

END

DATE FILMED
2-77

AFFDL-TR-76-86

(12) FC

SUBSONIC AND TRANSONIC SIMILARITY RULES FOR JET-FLAPPED WINGS

CONTROL CRITERIA BRANCH
FLIGHT CONTROL DIVISION

OCTOBER 1976

TECHNICAL REPORT AFFDL-TR-76-86
FINAL REPORT FOR PERIOD JANUARY 1975 - DECEMBER 1975

AIR FORCE FLIGHT DYNAMICS LABORATORY
AIR FORCE WRIGHT AERONAUTICAL LABORATORIES
AIR FORCE SYSTEMS COMMAND
WRIGHT-PATTERSON AIR FORCE BASE, OHIO 45433

NOTICE

When Government drawings, specifications, or other data are used for any purpose other than in connection with a definitely related Government procurement operation, the United States Government thereby incurs no responsibility nor any obligation whatsoever; and the fact that the government may have formulated, furnished, or in any way supplied the said drawings, specifications, or other data, is not to be regarded by implication or otherwise as in any manner licensing the holder or any other person or corporation, or conveying any rights or permission to manufacture, use, or sell any patented invention that may in any way be related thereto.

This report has been reviewed by the Information Office (OI) and is releasable to the National Technical Information Service (NTIS). At NTIS, it will be available to the general public, including foreign nations.

This technical report has been reviewed and is approved for publication.

Henry W. Woolard

Henry W. Woolard
Project Engineer

FOR THE COMMANDER

Evard H. Flinn

Evard H. Flinn
Chief Control Criteria Branch
Air Force Flight Dynamics Laboratory

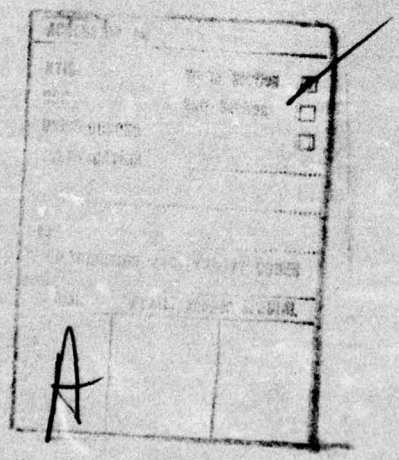

Copies of this report should not be returned unless return is required by security considerations, contractual obligations, or notice on a specific document.

AIR FORCE - 15 DECEMBER 76 - 150

SECURITY CLASSIFICATION OF THIS PAGE *(When Data Entered)*

REPORT DOCUMENTATION PAGE

READ INSTRUCTIONS BEFORE COMPLETING FORM

1. REPORT NUMBER: AFFDL-TR-76-86	2. GOVT ACCESSION NO.
3. RECIPIENT'S CATALOG NUMBER	
4. TITLE (and Subtitle): SUBSONIC AND TRANSONIC SIMILARITY RULES FOR JET-FLAPPED WINGS	5. TYPE OF REPORT & PERIOD COVERED: Final Report Jan — Dec 1975
	6. PERFORMING ORG. REPORT NUMBER
7. AUTHOR(s): Henry W. Woolard	8. CONTRACT OR GRANT NUMBER(s)
9. PERFORMING ORGANIZATION NAME AND ADDRESS: Air Force Flight Dynamics Laboratory (AFFDL/FGC) Air Force Wright Aeronautical Laboratories AFSC, W-PAFB, OH 45433	10. PROGRAM ELEMENT, PROJECT, TASK AREA & WORK UNIT NUMBERS: 62201F 82190120 01
11. CONTROLLING OFFICE NAME AND ADDRESS: (Same as above)	12. REPORT DATE: October 1976
	13. NUMBER OF PAGES: 57 pp
14. MONITORING AGENCY NAME & ADDRESS *(if different from Controlling Office)*	15. SECURITY CLASS. *(of this report)*: Unclassified
	15a. DECLASSIFICATION/DOWNGRADING SCHEDULE

16. DISTRIBUTION STATEMENT *(of this Report)*
Approved for public release; distribution unlimited.

17. DISTRIBUTION STATEMENT *(of the abstract entered in Block 20, if different from Report)*

18. SUPPLEMENTARY NOTES

19. KEY WORDS *(Continue on reverse side if necessary and identify by block number)*
Similarity/Jet Flaps
Jet-Flapped Wings
Similarity Rules
Subsonic Flow
Transonic Flow

20. ABSTRACT *(Continue on reverse side if necessary and identify by block number)*
Linear-subsonic and nonlinear-transonic similarity rules are derived for a finite-span jet-flapped wing with partial or full-span blowing. Although some subsonic rules previously have been published for jet-flapped wings, those presented herein are more general. The nonlinear transonic rules are new. The rules for both flow regimes employ a new jet-sheet compatibility condition that is second order relative to the jet-sheet internal flow and yields a jet-momentum coefficient similarity parameter differing from the conventional parameter in next page

DD FORM 1 JAN 73 1473 EDITION OF 1 NOV 65 IS OBSOLETE

012 070

SECURITY CLASSIFICATION OF THIS PAGE *(When Data Entered)*

bpg

20. Abstract (Contd)

cont.

that it includes the effect of the jet-supply pressure ratio. The examples presented show that the second-order effect is significant only for conditions under which a convergent jet nozzle chokes at a relatively low free-stream Mach number, say, less than 0.5. The relation of the present rules to previously published rules for both blown and unblown wings is discussed briefly. The experimental data available for validation of the linear rules is rather sparse and is plagued with uncertainties regarding wind-tunnel interference corrections. Nevertheless, some comparisons with experiment are made and fair agreement is achieved. These comparisons revealed that camber-line effects associated with blowing could be significant in transonic applications. There is no experimental data of appropriate configurational simplicity and of sufficient generally in parametric variations to permit validation of the nonlinear rules.

FOREWORD

This research was conducted by Henry W. Woolard of the Design Prediction Group, Control Criteria Branch, Flight Control Division, Air Force Flight Dynamics Laboratory, Wright-Patterson Air Force Base, Ohio. The work reported upon was performed in support of Work Unit Number 82190120.

TABLE OF CONTENTS

LIST OF FIGURES

LIST OF SYMBOLS

a	velocity of sound
A	wing aspect ratio
b	wing span
c	airfoil section chord
c_j	section isentropic momentum coefficient, $(\hat{\rho}_j \hat{U}_j h_j)\hat{U}_\infty/(\rho_\infty/2)U_\infty^2 c$
c_j''	section nozzle-exit momentum coefficient, $(\hat{\rho}_j \hat{U}_j h_j)\hat{U}_j/(\rho_\infty/2)U_\infty^2 c$
c_ℓ	section lift coefficient, $c_{\ell_\Gamma}+c_{\ell_R}$
$c_{\ell_\alpha}, c_{\ell_\delta} c_{\ell_\kappa}$	section lift coefficient derivatives with respect to α,δ,κ respectively
c_{ℓ_Γ}	section circulation lift coefficient
c_{ℓ_R}	section lift coefficient due to jet reaction
c_m	section pitching-moment coefficient, nose-up positive
C_{D_i}	induced-drag coefficient
C_L	wing lift coefficient, $C_{L_\Gamma}+C_{L_R}$
C_{L_Γ}	wing circulation lift coefficient
C_{L_R}	wing lift coefficient due to jet reaction
C_m	wing pitching moment coefficient about wing planform apex, nose-up positive, $C_{m_\Gamma}+C_{m_R}$
C_p	pressure coefficient, $(p-p_\infty)/(\rho_\infty/2)U_\infty^2$
$\mathcal{D}$	drag function
f_τ	wing thickness distribution function
f_κ	wing camber distribution function
h or h_{j_s}	jet-sheet thickness at an arbitrary location
h_j	jet-sheet thickness at nozzle (wing trailing edge)
H	section maximum camber height

LIST OF SYMBOLS (Contd)

I_G, I_F	see Eqs (57) and (58)
k	$(\gamma+1)M_\infty^2/U_\infty$
K_Π	jet compressibility factor (see Eqs 9 and 10)
L	lift function
M	Mach number
M	pitching-moment function
n,s	natural coordinates
p	static pressure
P	total pressure
P	pressure function
r	local radius of curvature in jet sheet (see Fig. 2)
R	radius of curvature at center of jet sheet (see Fig. 2)
R	gas constant
s	stretching factor (with appropriate subscript) as defined in Eq 14
S	wing area
S*	normalized wing area, $2S/bc_r$
t	maximum thickness of a wing section
u	local velocity parallel to x or s
$\hat{U}_j$	uniform jet velocity at nozzle (wing trailing edge)
$\hat{U}_\infty$	jet isentropic-expansion velocity corresponding to isentropic expansion of jet to free-stream static pressure
U_∞	free-stream velocity
x,y,z	cartesian coordinate system with positive x extending in the direction of the free-stream (see Fig. 1)
$\tilde{x},\tilde{y},\tilde{z}$	cartesian coordinate system in the transformed space according to Eq 14

LIST OF SYMBOLS (Contd)

x^*,y^*,z^*	normalized coordinates, $x/c_r, 2y/b, z/c_r$
$\|y_I\|, \|y_o\|$	inboard and outboard limits of spanwise blowing (see Fig 1)
α	angle of attack relative to the camber-line chord, i.e., the chord line joining the leading and trailing edges of the camber line
$\breve{\alpha}$	angle of attack relative to the chord line used in specifying the airfoil coordinates
$\breve{\alpha}'$	angle of attack relative to an arbitrary reference line
β_∞^2	$1-M_\infty^2$
γ	ratio of specific heats
δ_j	jet-flap deflection angle at wing trailing edge, measured positive downward relative to wing chord (see Fig. 1)
ϵ	see Eqs 19 and 20
Θ	local streamline slope in a plane y equals a constant, assuming negligible lateral flow (see Fig. 1)
Θ_i	upwash angle for induced-drag calculations
κ	section camber ratio, H/c
λ_c	ratio of tip-to-root chord
λ_t	ratio of tip-to-root thickness
λ_κ	ratio of tip-to-root maximum camber
Λ	wing sweepback angle
ρ	density
σ	optional parameter, may be τ, κ, α, Θ_j or δ_j
τ	wing-section thickness ratio, t/c
ϕ	perturbation velocity potential, $\Phi=U_\infty x+\phi$
Φ	total velocity potential
Ω	$\phi/U_\infty z$
ω	arbitrary constant (see text)

LIST OF SYMBOLS (Contd)

$( )_j$	denotes a quantity associated with the jet sheet at the wing trailing edge
$( )_{js}$	denotes a quantity associated with the jet sheet at any arbitrary location on the sheet
$( )_R$	denotes a quantity due to the jet reaction
$( )_o$	denotes a quantity on the centerline of the jet sheet
$( )_u, ( )_\ell$	denotes respectively the upper and lower stream surface for either the wing or jet sheet
$( )_r$	denotes the wing root chord
$( )_x, ( )_y, ( )_z$	denotes a partial derivative except when subscripting "s"
$( )_w$	denotes a wing quantity
$( )_\Gamma$	denotes a quantity due to the wing circulation lift
$( )_\infty$	denotes free-stream conditions
$( )_*$	denotes sonic conditions
$( )'$	denotes a perturbation quantity (except for α')
$(\tilde{})$	denotes a quantity in the transformed space according Eqs (14)
$(\hat{})$	denotes a quantity within the jet-sheet interior (see Fig. 2)
$\langle\ \rangle$	denotes a mean value

SECTION I

INTRODUCTION

With reference to Fig. 1, consider the flow about a finite-span pure[1]-jet-flapped wing with partial or full-span blowing[2] of the jet sheets. The motivation for study of this flow is the possible use of jet flaps for maneuvering combat aircraft at high subsonic and transonic speeds. This contrasts with the more conventional application of the jet-flap supercirculation principle wherein the jet sheets are employed to augment the lift of a mechanical flap during the takeoff or landing flight phase of an aircraft. In this latter application, compressibility effects are of secondary importance.

On the assumption of small flow perturbations and a restriction to wings without dihedral and twist, linear-subsonic and nonlinear-transonic similarity rules are derived herein for the subject flow. In developing these similarity rules a new jet-sheet compatibility condition, which is second order relative to the jet-sheet internal flow, is derived. The new compatibility condition yields a jet-momentum coefficient similarity parameter differing from the conventional parameter in that it includes the effect of the jet-supply pressure ratio. In application of the similarity laws, particular attention is given to camber-line effects which heretofore have been unimportant in applications involving jet-augmented mechanical flaps.

The nonlinear transonic similarity rules derived herein for jet-flapped wings are new (to the best of the author's knowledge). For the linear-subsonic case, however, similarity laws for jet-flapped wings previously have been presented by Siestrunk (Ref. 1), Levinsky (Ref. 2), and Elzweig (Ref. 3). Each of these investigators employs a different

[1] That is, a wing employing jet sheets alone, unassisted by mechanical devices such as flaps or ailerons.

[2] For convenience in discussion, reference to a "blown" or "unblown" wing will connote, respectively, a wing with or without the jet flaps operating.

scaling law, and only Levinsky considers the finite-span wing; the other treatments are for two-dimensional flow. The present treatment is more general than the foregoing ones in that it applies to both two- and three-dimensional wings, allows for the selection of the scaling law most appropriate to the particular problem under consideration, and includes a second-order scaling of the jet internal flow that accounts for the jet-supply pressure ratio. The laws employed herein reduce to those of the aforementioned investigators upon appropriate selection of the parameters.

As a consequence of the assumption of small perturbations, application of the present results obviously is limited to small thickness and camber ratios, small angles of attack, and small jet-deflection angles.

SECTION II

ANALYSIS

For an untwisted wing with camber and thickness, but without dihedral, the geometry may be given by

$$z_w^* = \sigma F\left(x^*, y^*; g_i^{(\tau)}, g_i^{(\kappa)}, \frac{\tau_r}{\sigma}, \frac{\kappa_r}{\sigma}, \frac{\alpha}{\sigma}\right)$$

where

$$F \equiv \pm \frac{\tau_r}{\sigma} f_\tau(x^*, y^*; g_i^{(\tau)}) + \frac{\kappa_r}{\sigma} f_\kappa(x^*, y^*; g_i^{(\kappa)}) - \frac{\alpha}{\sigma} x^* \qquad (1)$$

with a specified spanwise blowing distribution given by

$$c_j = c_j\,(y^*_j)$$
$$\delta_j = \delta_j\,(y^*_j) \qquad (2)$$

The g_i quantities in Eq. 1 are the nondimensional geometric parameters required to define the specific wing geometry being considered, with

$$g_i^{(\tau)} = g_1^{(\tau)}, g_2^{(\tau)}, \text{-------} g_{n_\tau}^{(\tau)}, \quad i = 1, 2, 3, \text{---} n_\tau$$
$$g_i^{(\kappa)} = g_1^{(\kappa)}, g_2^{(\kappa)}, \text{-------} g_{n_\kappa}^{(\kappa)}, \quad i = 1, 2, 3, \text{---} n_\kappa \qquad (3)$$

For some configurations, some of the $g_i^{(\tau)}$, $g_i^{(\kappa)}$ parameters may be identical (e.g., $g_1^{(\tau)} = g_1^{(\kappa)}$. The parameter σ may be selected to be any one of the parameters τ_r, κ_r, α, Θ_j or δ_j depending upon the type of problem under consideration.

For definiteness, it is of interest to apply the foregoing relations to a specific class of wings designated as "trapezoidal." A "trapezoidal wing" is defined herein as a wing (without dihedral or twist) for which the half-span planform is a trapezoid with the root and tip chords parallel, the wing-section geometries affine to each other at varying spanwise stations, and the section characteristic dimensions (chord, thickness, camber height, etc.) vary linearly in the spanwise direction.

For this class of wings, the functions in Eq. 1 have the form

$$\left.\begin{aligned} f_\tau &= f_\tau(x^*, y^*; A \tan \Lambda, \lambda_c, \lambda_t) \\ f_\kappa &= f_\kappa(x^*, y^*; A \tan \Lambda, \lambda_c, \lambda_\kappa) \end{aligned}\right\} \quad (4)$$

where

$$\left.\begin{aligned} g_1^{(\tau)} &= g_1^{(\kappa)} = A \tan \Lambda \\ g_2^{(\tau)} &= g_2^{(\kappa)} = \lambda_c \\ g_3^{(\tau)} &= \lambda_t, \; g_3^{(\kappa)} = \lambda_\kappa \\ g_i^{(\tau)} &= g_i^{(\kappa)} = 0; \; i > 3 \end{aligned}\right\} \quad (5)$$

Explicit forms of the f_τ- and f_κ - functions are not displayed since they serve no useful purpose here. They are easily derived, however, if required.

Deflected ailerons and flaps may be treated by introducing additional "camber-like" functions.

The governing partial differential equation for the perturbation velocity potential (Ref. 5) is

$$\beta_\infty^2 \frac{\partial^2 \phi}{\partial x^2} + \frac{\partial^2 \phi}{\partial y^2} + \frac{\partial^2 \phi}{\partial z^2} = jk \frac{\partial \phi}{\partial x} \frac{\partial^2 \phi}{\partial x^2} \quad (6)$$

where for linear subsonic compressible flow $j = 0$, and for nonlinear transonic flow $j = 1$.

The shock-wave compatibility condition (Ref. 5) is

$$\beta_\infty^2 (\Delta\phi_x)^2 + (\Delta\phi_y)^2 + (\Delta\phi_z)^2 = k \, (\tfrac{1}{2})(\phi_{x_1} + \phi_{x_2})(\Delta\phi_x)^2 \quad (7)$$

where the subscripts x, y, and z denote partial derivatives, and Δ denotes a jump in the modified quantity such that if "1" and "2" denote, respectively, upstream and downstream conditions relative to the shock $\Delta\phi_x = \phi_{x_1} - \phi_{x_2}$, etc.

If the lateral-flow velocity perturbations are assumed to be neglible compared to the vertical and longitudinal ones, the jet-sheet compatibility condition (see Appendix A) is

$$\frac{1}{U_\infty}\left(\frac{\partial\phi}{\partial x}\right)_{z=0} = \frac{c}{4}\left(\frac{\partial\Theta_{js}}{\partial x}\right) K_\pi c_j \tag{8}$$

where

$$K_\pi = 1 \qquad \text{for} \qquad (\hat{P}/p_\infty \leq \hat{P}/\hat{p}_*) \tag{9}$$

$$K_\pi = 1 - \frac{1}{2\gamma}\left(1 - \frac{\hat{P}/\hat{p}_*}{\hat{P}/p_\infty}\right) \qquad \text{for} \qquad (\hat{P}/\hat{p}_* \leq \hat{P}/p_\infty \leq 5 \tag{10}$$

For $\gamma = 1.4$, $P/p_* = 1.893$

The boundary conditions at $x = -\infty$ and $y = \pm\infty$ are

$$\phi_x = \phi_y = \phi_z = 0 \tag{11}$$

The wing surface boundary condition is

$$\left(\frac{\partial\phi}{\partial z}\right)_{z=0} = U_\infty \sigma \frac{\partial}{\partial x^*} F\left(x^*, y^*; \frac{\tau_r}{\sigma}, \frac{\kappa_r}{\sigma}, \frac{\alpha}{\sigma}\right) \tag{12}$$

The jet-sheet boundary condition is

$$\Theta_{js}\ (x^*, y^*, 0) = (\partial\phi/\partial z)_{z=0}/U_\infty \tag{13}$$

We now introduce the transformations

$$\left.\begin{aligned} &\tilde{x} = s_x x,\ \tilde{y} = s_y y,\ \tilde{z} = s_z z,\ \tilde{\phi} = s_\phi \phi \\ &\tilde{U}_\infty = s_u U_\infty,\ \tilde{\beta}_\infty = s_\beta \beta_\infty,\ (\tilde{U}_\infty \tilde{k}) = s_k\ (U_\infty k) \end{aligned}\right\} \tag{14}$$

Flow similarity is achieved by determining appropriate values of the s-stretching factors as dictated by the governing equations and boundary conditions.

The boundary conditions specified by Eq. 11 are obviously preserved by the transformations of Eq. 14.

We consider first the constraints imposed on the stretching factors by the governing partial differential equation, Eq. 6, and the shock compatibility condition, Eq. 7. Applying the transformations of Eq. 14 yields the governing differential equation:

$$\frac{s_x^2}{s_\beta^2 s_\phi}\,\tilde{\beta}_\infty^2\,\frac{\partial^2\tilde{\phi}}{\partial\tilde{x}^2}+\frac{s_y^2}{s_\phi}\frac{\partial^2\tilde{\phi}}{\partial\tilde{y}^2}+\frac{s_z^2}{s_\phi}\frac{\partial^2\tilde{\phi}}{\partial\tilde{z}^2}=j\,\frac{s_u s_x^3}{s_k s_\phi^2}\,\tilde{k}\,\frac{\partial\tilde{\phi}}{\partial\tilde{x}}\frac{\partial^2\tilde{\phi}}{\partial\tilde{x}^2} \tag{15}$$

and for the shock compatibility condition

$$\frac{s_x^2}{s_\beta^2 s_\phi^2}\,\tilde{\beta}_\infty^2\,(\Delta\tilde{\phi}_x)^2+\frac{s_y^2}{s_\phi^2}\,(\Delta\tilde{\phi}_y)^2+\frac{s_z^2}{s_\phi^2}\,(\Delta\tilde{\phi}_z)^2=\frac{s_u s_x^3}{s_k s_\phi^3}\,\tilde{k}\,\left(\frac{\tilde{\phi}_{x_1}+\tilde{\phi}_{x_2}}{2}\right)(\Delta\tilde{\phi}_x)^2 \tag{16}$$

Comparison of Eqs. 6 and 15 for the linear and nonlinear problems and Eqs. 7 and 16 for the nonlinear problems yields the following conditions for flow similarity

Linear

$$\frac{s_x^2}{s_\beta^2}=s_y^2=s_z^2$$

$$\frac{s_x^2}{s_k}\left(\frac{s_u s_x}{s_\phi}\right)=\text{an arbitrary constant} \tag{17a}$$

Nonlinear

$$\frac{s_x^2}{s_\beta^2}=s_y^2=s_z^2=\frac{s_x^2}{s_k}\left(\frac{s_u s_x}{s_\phi}\right) \tag{17b}$$

For the linear case, the freedom in choice of the parametric combination $(s_u s_x^3/s_k s_\phi)$ introduces the option of an additional degree of freedom in the scaling. This option is a well-known property of subsonic scaling laws (see, e.g., Refs. 5 and 6).

Equations 17a and 17b may be generalized in the following manner

$$\frac{s_x^2}{s_\beta^2}=s_y^2=s_z^2=\frac{s_x^2}{\tilde{\epsilon}/\epsilon}\left(\frac{s_u s_x}{s_\phi}\right) \tag{18}$$

where

$$\tilde{\epsilon}/\epsilon = \text{an arbitrary constant} \qquad \text{(Linear)} \qquad (19)$$

$$\tilde{\epsilon}/\epsilon = (\tilde{U}_\infty \tilde{k}/U_\infty k) \qquad \text{(Non-linear)} \qquad (20)$$

For the linear case, the ratio $(\tilde{\epsilon}/\epsilon)$ is analogous to the ratio $(\tilde{\lambda}/\lambda)$ employed by Spreiter (Ref. 5). The two ratios[3] are related by

$$(\tilde{\epsilon}/\epsilon) = (\tilde{\beta}_\infty^2 \tilde{\lambda}/\beta_\infty^2 \lambda).$$

Equating the first and third terms in Eq. 18 yields $s_x = s_\beta s_z$, from which it may be determined that

$$\left(\frac{s_u s_x}{s_\phi}\right) = s_\beta \left(\frac{s_u s_z}{s_\phi}\right) \qquad (21)$$

In the analyses which follow, (s_u/s_ϕ) always appears in one of the parenthetical combinations shown in Eq. 21. The stretching factors s_u and s_ϕ therefore need not be determined separately and the quantities $(s_u s_x/s_\phi)$ and $(s_u s_z/s_\phi)$ may be treated as unknown parameters.

Substituting Eq. 21 in Eq. 18 yields, with $\Omega/\Omega = s_\phi/s_u s_z$

$$\frac{s_x^2}{s_\beta^2} = s_y^2 = s_z^2 = \frac{s_x^2 s_\beta}{(\tilde{\epsilon}/\epsilon)(\tilde{\Omega}/\Omega)} \qquad (22)$$

The relation Eq. 22 defines three equations relating the stretching factors. This set of equations may have a variety of forms, depending upon the algebraic manipulations performed. The forms used herein are

$$s_y \, (\tilde{\epsilon}\tilde{\Omega}/\epsilon\Omega)^{1/3} = s_x \qquad (23)$$

$$s_z \, (\tilde{\epsilon}\tilde{\Omega}/\epsilon\Omega)^{1/3} = s_x \qquad (24)$$

$$\tilde{\Omega}/\Omega = (\tilde{\beta}_\infty/\beta_\infty)^3 (\epsilon/\tilde{\epsilon}) \qquad (25)$$

[3]The symbol λ is Spreiter's λ, not the λ used herein

The principal linear dimensions of the original and transformed wings are related by

$$\tilde{c}_r = s_x c_r;\ \tilde{b} = s_y b;\ \tilde{t}_r = s_z t_r$$
$$\tilde{y}_I = s_y y_I;\ \tilde{y}_o = s_y y_o \tag{26}$$

yielding

$$\tilde{x}^* = x^*;\ \tilde{y}^* = y^*;\ (\tilde{\varepsilon}\tilde{\Omega})^{1/3}\tilde{z}^* = (\varepsilon\Omega)^{1/3} z^*$$
$$\tilde{y}_I^* = y_I^*;\ \tilde{y}_o^* = y_o^* \tag{27}$$

The transformation relations, Eq. 14, and the similarity conditions of Eqs. 17a and 17b also yield

$$(\tan \tilde{\Lambda})/\tilde{\beta}_\infty = (\tan \Lambda)/\beta_\infty \tag{28}$$

$$\tilde{\beta}_\infty \tilde{A} = \beta_\infty A \tag{29}$$

Any one of the parameters s_x, s_y or s_z in Eq. 26 may be assigned an arbitrary value. For unit values of s_x, s_y, and s_z respectively, Eq. 26 indicates that wings of identical root chord, span, or root thickness respectively are being compared in the original and transformed spaces. A common selection is $s_x = 1.0$

To achieve manageable results, it is necessary to assume that $\tilde{f}_\tau = f_\tau$, $\tilde{f}_\kappa = f_\kappa$, and $\tilde{F} = F$. That is, the analysis is confined to families of wings defined by these constraints. The wing geometry in the transformed space then becomes

$$\tilde{z}_w^* = \tilde{\sigma} F\left(\tilde{x}^*, \tilde{y}^*; \tilde{g}_i^{(\tilde{\tau})}, \tilde{g}_i^{(\tilde{\kappa})}, \frac{\tilde{\tau}_r}{\tilde{\sigma}}, \frac{\tilde{\kappa}_r}{\tilde{\sigma}}, \frac{\tilde{\alpha}}{\tilde{\sigma}}\right) \tag{30}$$

where

$$F \equiv \pm \frac{\tilde{\tau}_r}{\tilde{\sigma}} f_{\tilde{\tau}}(\tilde{x}^*, \tilde{y}^*; \tilde{g}_i^{(\tilde{\tau})}) + \frac{\tilde{\kappa}_r}{\tilde{\sigma}} f_\kappa\ (\tilde{x}^*, \tilde{y}^*; \tilde{g}_i^{(\tilde{\kappa})}) - \frac{\tilde{\alpha}}{\tilde{\sigma}}\tilde{x}^* \tag{31}$$

with

$$\tilde{c}_j = \tilde{c}_j\ (\tilde{y}_j^*)$$
$$\tilde{\delta}_j = \tilde{\delta}_j\ (\tilde{y}_j^*) \tag{32}$$

The equality of the f's requires that

$$\tilde{g}_i^{(\tilde{\tau})} = g_i^{(\tau)}; \quad \tilde{g}_i^{(\tilde{\kappa})} = g_i^{(\kappa)} \tag{33}$$

where for trapezoidal wings the g_i's are defined by Eq 5. The equality of the F's, in combination with the equality of the f's, requires that

$$\tilde{\tau}_r/\tilde{\sigma} = \tau_r/\sigma \tag{34}$$

$$\tilde{\kappa}_r/\tilde{\sigma} = \kappa_r/\sigma \tag{35}$$

$$\tilde{\alpha}/\tilde{\sigma} = \alpha/\sigma \tag{36}$$

For trapezodial wings, the invariances specified by Eqs. 33 require that

$$\tilde{A} \tan \tilde{\Lambda} = A \tan \Lambda \tag{37}$$

$$\tilde{\lambda}_c = \lambda_c, \; \tilde{\lambda}_t = \lambda_t, \; \tilde{\lambda}_\kappa = \lambda_\kappa \tag{38}$$

It is apparent that the transformations of Eq. 14 are consistent with the conditions of Eqs. 37 and 38 which are a consequence of restricting the analysis to a family of wings. Also note that Eq. 37 is equivalent to the pair of Eqs. 28 and 29.

The boundary condition on the wing in the transformed space is given by

$$\left(\frac{\partial \phi}{\partial \tilde{z}}\right)_{\tilde{z}=0} = \tilde{U}_\infty \, \tilde{\sigma} \, \frac{\partial}{\partial \tilde{x}^*} \, F(\tilde{x}^*, \; \tilde{y}^*; \; \text{------}) \tag{39}$$

Applying the transformations of Eq. 14 to the boundary condition in the original space yields

$$\frac{s_z}{s_\phi} \left(\frac{\partial \tilde{\phi}}{\partial \tilde{z}}\right)_{\tilde{z}=0} = \frac{\tilde{U}_\infty}{s_u} \, \sigma \, \frac{\partial}{\partial x^*} \, F(x^*, \; y^*; \; \text{------}) \tag{40}$$

Equations 39 and 40 are similar if $(\tilde{\sigma}/\sigma) = s_\phi/s_u s_z)$. This condition, an invariant of the transformation, may be written as $(\tilde{\Omega}/\tilde{\sigma}) = (\Omega/\sigma)$. In applying the similarity laws, the aforementioned invariant is frequently employed in the form

$$(\tilde{\Omega}/\tilde{\sigma})^\omega = (\Omega/\sigma)^\omega \tag{41}$$

where the value of ω is arbitrarily selected to achieve a particular desired form for the invariant parameters in the final formation of the similarity rules. Common choices are (-1) and (2/3) respectively for subsonic and transonic flows.

Assuming negligible lateral flow, the streamline slopes in the two spaces are

$$\Theta = \frac{\partial\phi/\partial z}{U_\infty} \tag{42}$$

$$\tilde{\Theta} = \frac{\partial\tilde{\phi}/\partial\tilde{z}}{\tilde{U}_\infty} = \frac{s_\phi}{s_u s_z}\frac{\partial\phi/\partial z}{U_\infty} = \frac{\tilde{\Omega}}{\Omega}\frac{\partial\phi/\partial z}{U_\infty} \tag{43}$$

yielding the result $(\tilde{\Omega}/\tilde{\Theta}) = (\Omega/\Theta)$, where, as for Eq. 41, we employ the form

$$(\tilde{\Omega}/\tilde{\Theta})^\omega = (\Omega/\Theta)^\omega \tag{44}$$

Since the jet sheet is a stream surface, Eq. 44 applies to the jet-sheet slopes Θ_{js} and $\tilde{\Theta}_{js}$. A basic parameter for the jet sheet, however, is the slope, Θ_j, at the wing trailing edge. Applying Eq. 44 to Θ_j and $\tilde{\Theta}_j$ yields

$$(\tilde{\Omega}/\tilde{\Theta}_j)^\omega = (\Omega/\Theta_j)^\omega \tag{45}$$

where

$$\Theta_j = -(\alpha + \delta_j),\ \tilde{\Theta}_j = -(\tilde{\alpha} + \tilde{\delta}_j) \tag{46}$$

Equation 46 may be written as

$$\Theta_j = -\delta_j\left(\frac{\alpha}{\delta_j} + 1\right),\ \tilde{\Theta} = -\tilde{\delta}_j\left(\frac{\tilde{\alpha}}{\tilde{\delta}_j} + 1\right)$$

For $\sigma = \delta_j$, Eq. 36 yields

$$\tilde{\alpha}/\tilde{\delta}_j = \alpha/\delta_j$$

The above equations yield

$$\tilde{\Theta}_j/\Theta_j = \tilde{\delta}_j/\delta_j \qquad (\sigma = \delta_j) \tag{47}$$

When σ is selected to be δ_j, an optional form for Eq. 45 is, therefore,

$$(\tilde{\Omega}/\tilde{\delta})^{\omega} = (\Omega/\delta_j)^{\omega} \qquad (\sigma = \delta_j) \tag{48}$$

The compatibility condition for the jet sheet in the original space is given by Eq. 8; in the transformed space it is

$$\frac{1}{\tilde{U}_\infty}\left(\frac{\partial\tilde{\phi}}{\partial\tilde{x}}\right)_{\tilde{z}=0} = \frac{\tilde{c}}{4}\left(\frac{\partial\tilde{\Theta}_{js}}{\partial\tilde{x}}\right)\tilde{K}_\pi\tilde{c}_j \tag{49}$$

Applying the transformations of Eqs. 14 and 44 to Eq. 8 yields

$$\frac{(1/s_\phi)}{(1/s_u)\tilde{U}_\infty(1/s_x)}\left(\frac{\partial\tilde{\phi}}{\partial\tilde{x}}\right)_{\tilde{z}=0} = \frac{\tilde{c}}{4}\frac{1}{s_x}\frac{1}{(s_\phi/s_u s_z)}\, s_x \left(\frac{\partial\tilde{\Theta}_{js}}{\partial\tilde{x}}\right) K_\pi c_j$$

or

$$\frac{1}{\tilde{U}_\infty}\left(\frac{\partial\tilde{\phi}}{\partial\tilde{x}}\right)_{\tilde{z}=0} = \frac{\tilde{c}}{4}\frac{s_z}{s_x}\left(\frac{\partial\tilde{\Theta}_{js}}{\partial\tilde{x}}\right) K_\pi c_j \tag{50}$$

The ratio (s_z/s_x) may be obtained from Eq. 24. Substituting in Eq. 50 yields

$$\frac{1}{\tilde{U}_\infty}\left(\frac{\partial\tilde{\phi}}{\partial\tilde{x}}\right)_{\tilde{z}=0} = \frac{\tilde{c}}{4}\left(\frac{\Omega\varepsilon}{\tilde{\Omega}\tilde{\varepsilon}}\right)^{1/3}\left(\frac{\partial\tilde{\Theta}_{js}}{\partial\tilde{x}}\right) K_\pi c_j \tag{51}$$

From Eqs. 49 and 51

$$(\tilde{\varepsilon}\tilde{\Omega})^{1/3}\tilde{K}_\pi\tilde{c}_j = (\varepsilon\Omega)^{1/3}K_\pi c_j \tag{52}$$

where, from Eqs. 25, 41, 45, and 48, the ratio $(\tilde{\Omega}/\Omega)$ required for Eq. 52 is given by any one of the following equations

$$\tilde{\Omega}/\Omega = \begin{cases} \tilde{\beta}_\infty^{\,3}\varepsilon/\beta_\infty^{\,3}\tilde{\varepsilon} \\ \tilde{\sigma}/\sigma \\ \tilde{\Theta}_j/\Theta_j \end{cases} \tag{53}$$

Equations 52 and 53 are the invariant conditions for the jet-momentum coefficient. Note that if σ is selected to be other than δ_j or Θ_j

(with $\tilde{\sigma}$ selected correspondingly), Eq. 53 permits three optional choices for $\tilde{\Omega}/\Omega$, but if σ is selected to be δ_j or Θ_j (with $\tilde{\sigma}$ selected correspondingly) only two options are available for $\tilde{\Omega}/\Omega$.

The relation between the pressure coefficients at corresponding points in the two spaces is given by

$$\tilde{C}_p = -\frac{2}{\tilde{U}_\infty}\left(\frac{\partial\tilde{\phi}}{\partial\tilde{x}}\right) = \left(\frac{s_\phi}{s_u s_x}\right)\left(-\frac{2}{U_\infty}\frac{\partial\phi}{\partial x}\right)$$

or

$$\tilde{C}_p = \left(\frac{s_\phi}{s_u s_x}\right) C_p \tag{54}$$

The factor $(s_\phi/s_u s_x)$ in Eq. 54 can be written as $(s_\phi/s_u s_x)^{2/3}(s_\phi/s_u s_x)^{1/3}$ and appropriately manipulated to give

$$\left(\frac{s_\phi}{s_u s_x}\right) = \left(\frac{\tilde{\Omega}}{\Omega}\right)^{2/3}\left(\frac{\varepsilon}{\tilde{\varepsilon}}\right)^{1/3} \tag{55}$$

Substituting Eq 55 in Eq. 54 and indicating the functional dependence of the pressure coefficient yields

$$\begin{aligned}(\varepsilon/\Omega^2)^{1/3} C_p \left[x^*,\ y^*,\ (\varepsilon\Omega)^{1/3} z^*;\ I_G,\ I_F\right] \\ = (\tilde{\varepsilon}/\tilde{\Omega}^2)^{1/3}\tilde{C}_p \left[\tilde{x}^*,\ \tilde{y}^*,\ (\tilde{\varepsilon}\tilde{\Omega})^{1/3}\tilde{z}^*;\ \tilde{I}_G,\ \tilde{I}_F\right]\end{aligned} \tag{56}$$

where

$$I_G \equiv y^*_I,\ y^*_o,\ \lambda_c,\ \lambda_t,\ \lambda_\kappa \tag{57}$$

$$I_F \equiv ((\tan\Lambda)/\beta_\infty),\ \beta_\infty A,\ \tau_r/\sigma,\ \kappa_r/\sigma,\ \alpha/\sigma,\ (\Omega/\sigma)^\omega,\ \underline{(\Omega/\Theta_j)^\omega},\ (\varepsilon\Omega)^{1/3}(K_\pi c_j) \tag{58}$$

and K_π is given by Eqs. 9 and 10. The parameter σ may be selected as any one of the parameters τ_r, κ_r, α, Θ_j, or δ_j depending upon the type of problem under consideration. The form of the parameter ε (and hence $\tilde{\varepsilon}$) is arbitrary for subsonic linear flow, and, in accordance with Eq. 20, is $\varepsilon = U_\infty k$ ($\tilde{\varepsilon} = \tilde{U}_\infty \tilde{k}$) for nonlinear transonic flow. The optional choices for the form of Ω (and hence $\tilde{\Omega}$) are specified by Eq. 53. The value of ω is arbitrary and depends upon the type of problem under consideration.

Common selections for ω are (-1) and (2/3) respectively for subsonic and transonic flow. When σ is selected to be Θ_j or δ_j, the underlined parameter in Eq. 58 is omitted. Additionally, a selection for σ that yields unity for any one of the ratioed parameters in Eq. 58 indicates a lack of an invariance constraint on that ratio. The invariants I_G and I_F are separately identified since the I_G invariants are purely geometric at all times, whereas the I_F quantities may consist of a mixture of geometric and fluidynamic invariants, the exact nature of which depends upon the specific forms selected for σ, Ω, and ε. There is no unique combination of the similarity parameters appearing in Eqs. 56 and 58. The parameters shown may be rearranged to give a wide variety of combinations by appropriate manipulation of Eqs. 34, 36, 37 and 53 (noting the equivalence of the ratios on the right-hand side of Eq. 53.) Such a procedure is permissible providing the total number of invariant parameters remains unchanged in any rearrangement.

The following aerodynamic coefficients are defined

$$C_L = C_{L_\Gamma} + C_{L_R} \tag{59}$$

$$C_{L_\Gamma} = \frac{bc_r}{2S} \iint_{S^*} (C_{p_\ell} - C_{p_u}) dx^* dy^* \tag{60}$$

$$C_{L_R} = -\frac{bc_r}{2S} \int_{-1}^{1} c_j \, \Theta_j \, \left(\frac{c}{c_r}\right) dy^* \tag{61}$$

$$C_{D_i} = -\Theta_i \, C_L \tag{62}$$

$$C_m = C_{m_\Gamma} + C_{m_R} \tag{63}$$

$$C_{m_\Gamma} = -\frac{bc_r}{2S} \iint_{S^*} x^* \, (C_{p_\ell} - C_{p_u}) dx^* dy^* \tag{64}$$

$$C_{m_R} = \frac{bc_r}{2S} \int_{-1}^{1} x^*_j \, c_j \, \Theta_j \, (\frac{c}{c_r}) dy^* \tag{65}$$

where $(-\Theta_i)$ is an appropriate downwash angle and the small-angle assumption $(\sin\Theta_j = \Theta_j)$ has been employed in the jet-reaction coefficients.

Application of the similarity rules yields the following results

$$C_p(x^*, y^*, 0) = (\frac{\Omega^2}{\varepsilon})^{1/3} P \, (x^*, y^*, 0; I_G, I_F) \tag{66}$$

$$C_{L_\Gamma} = (\frac{\Omega^2}{\varepsilon})^{1/3} L_\Gamma \, (I_G, I_F) \tag{67}$$

$$C_{L_R} = (\frac{\Omega^2}{\varepsilon})^{1/3} L_R \, (I_G, I_F) \tag{68}$$

$$C_L = (\frac{\Omega^2}{\varepsilon})^{1/3} L \, (I_G, I_F) \tag{69}$$

$$C_{D_i} = (\frac{\Omega^5}{\varepsilon})^{1/3} D_i \, (I_G, I_F) \tag{70}$$

$$C_{m_\Gamma} = (\frac{\Omega^2}{\varepsilon})^{1/3} M_\Gamma \, (I_G, I_F) \tag{71}$$

$$C_{m_R} = (\frac{\Omega^2}{\varepsilon})^{1/3} M_R \, (I_G, I_F) \tag{72}$$

$$C_m = (\frac{\Omega^2}{\varepsilon})^{1/3} M \, (I_G, I_F) \tag{73}$$

where I_G and I_F are given by Eqs. 57 and 58, respectively, and $L = L_\Gamma + L_R$ and $M = M_\Gamma + M_R$.

Since in the linear case the form of ε may be selected arbitrarily, it is of interest to examine the consequences of several choices for this parameter. For $\varepsilon = \Omega^2$ ($\tilde{\varepsilon} = \tilde{\Omega}^2$), Eq. 56 shows that the pressure coefficients at affinely related points in the original and transformed spaces are identical. For $\varepsilon = \beta_\infty{}^3$, Eq. 25 shows that $\Omega = \tilde{\Omega}$, from which it follows from Eq. 41 that $\sigma = \tilde{\sigma}$ and, from Eq. 45, that $\Theta_j = \tilde{\Theta}_j$. Finally, equations 34, 35, and 36 show that the thickness ratios, camber ratios, and angles of attack are identical in the original and transformed spaces. For $\varepsilon = U_\infty k$, Eqs. 19 and 20 show that the similarity parameters will be identical for both linear and nonlinear flows. This allows theoretical solutions of the linear and nonlinear flows to be plotted on the same set of graphs in terms of the same set of parameters. The two theories would, of course, yield different curves on such plots. The curves for linear theory would be valid for purely subsonic flows, but may or may not be valid for transonic flows. The curves for nonlinear transonic flow would be valid not only for transonic, but for subsonic and supersonic small-perturbation flows as well.

When the foregoing similarity rules are applied to two-dimensional flows, the finite-span dependent terms are obviously omitted.

SECTION III

COMPARISON WITH PREVIOUS ANALYSES

For the unblown wing there is no dependence upon c_j and δ_j, and the foregoing results may be shown to reduce to those of various investigators by appropriate selection of Ω, ε, and σ, and, perhaps, some additional manipulation of the invariants as previously noted. The results of Spreiter (Appendix B, Ref. 5), for example, may be obtained by using Eqs. 28 and 29 to replace A tan Λ with β_∞ tan Λ and taking $\omega=1$, $\Omega=\beta_\infty^{\,3}/\varepsilon$, $\varepsilon=\beta_\infty^{\,2}\lambda$, and $\sigma=\tau_r$ for linear flow; and taking $\omega=1/3$, $\Omega=\tau_r$, $\varepsilon=\kappa U_\infty$, and $\sigma=\tau_r$ for nonlinear flow.

As mentioned previously, there are no other similarity analyses (to the best of this writer's knowledge) for nonlinear jet-flapped-wing flow, hence comparisons will be limited to linear flow. Comparisons will be made with the work of Siestrunk (Ref. 1), Levinsky (Ref. 2) and Elzweig (Ref. 3). Each of these investigators uses a different scaling law. There are, perhaps, other works, but the foregoing provide sufficient variety for the present purposes. Among the aforementioned analyses, Levinsky's is the only one applicable to finite-span wings; the other treatments are for two-dimensional flow. None of the analyses include second-order terms in the jet internal flow; hence, in comparing with the present work, the parameter K_π will be taken as unity.

Siestrunk employs a scaling that maintains equal angles of attack and jet deflection angles in the original and transformed spaces. Levinsky employs Göthert's scaling (see Ref. 6), which is applicable also to axially symmetric flow. Elzweig employs a scaling for which the wing-surface pressure coefficients are equal at affinely related points in the original and transformed spaces.

The results of Siestrunk are obtained by taking $\tau_r=\kappa_r=0$, $\sigma=\alpha$, $\varepsilon=\beta_\infty^{\,3}$, $\Omega=1$, and $\omega=-1$. Those of Levinsky are obtained by taking $\tau_r=\kappa_r=0$, $\sigma=\alpha$, $\varepsilon=\beta_\infty^{\,4}$, $\Omega=\beta_\infty^{\,-1}$, $\omega=-1$. The results of Elzweig are obtained by taking $\tau_r=\kappa_r=0$, $\sigma=\alpha$, $\varepsilon=\beta_\infty^{\,2}$, $\Omega=\beta_\infty$ and $\omega=-1$.

SECTION IV

COMPARISON WITH EXPERIMENT

As noted previously, for jet-flapped wings there is no experimental data of appropriate configurational simplicity and of sufficient generality in parametric variations to permit validation of the nonlinear rules (to the knowledge of this writer). The data available for validation of the linear rules is rather sparse and is plagued with uncertainties regarding wind-tunnel wall corrections. Nevertheless some limited comparisons are made in this section. The data sources selected for comparison are: (1) Air Force/Northrop tests (Refs. 8 and 9), (2) Air Force/Convair/Canadian tests (Refs. 10, 11, 12, and 13), and (3) French O.N.E.R.A tests (Ref. 14). The first two test series are for two-dimensional airfoils, whereas the third is for a finite-aspect-ratio wing employing a semispan test arrangement.

AIR FORCE/NORTHROP TESTS

These tests (Refs. 8 and 9) were conducted at the Arnold Engineering Development Center (AEDC) in the 4T wind tunnel which has a 4-x 4-foot porous-wall test section. The model tested has a modified NACA 64A406 airfoil section, a 10-inch chord, a 20-inch span and was mounted between two large end plates. Tests were conducted at Mach numbers of 0.70, 0.80, 0.85, 0.90 and 0.95 and at effective jet-flap deflection angles (δ_j) of 0, 35, 55, and 88 degrees. Forces and moments were not measured directly, but were deduced from measured surface pressures. The data presented in Refs. 8 and 9 was not corrected[4] for tunnel or end-plate interference effects. Therefore, for the present comparisons an approximate correction is derived in Appendix B of this report.

Since the camber line of the airfoil used in these tests is almost parabolic, the parabolic camber-line relations of Appendix C are used in estimating the airfoil aerodynamics. The applicable incompressible lift

[4]Private communication with the test conductor.

coefficient relation is given by Eq. 5 in Appendix C. Taking $\varepsilon = \beta_\infty^3$, $\Omega = 1$, $\sigma = \alpha$, and $\omega = -1$ in Eq. 69 yields, for the subsonic similarity relation,

$$c_\ell = \frac{1}{\beta_\infty}\left[\kappa c_{\ell_\kappa}\,(\beta_\infty K_\pi c_j) + \alpha c_{\ell_\alpha}\,(\beta_\infty K_\pi c_j) + \delta_j c_{\ell_{\delta_i}}\,(\beta_\infty K_\pi c_j)\right] \qquad (74)$$

The consequences of Eq. 74 are compared with experiment in Fig. 3. The 35-degree jet-flap deflection case was selected for comparison since the theory is more strictly applicable to smaller jet-flap angles. The experimental data shown is for a constant geometrical angle of attack[5], which differs from the actual aerodynamic angle of attack due to tunnel interference effects. It would have been preferable to present the experimental results at a constant aerodynamic angle of attack, but the data of Refs. 8 and 9 for $\delta_j = 35°$ was too meager[6] to permit construction of the required cross plots. The theoretical results directly comparable to experiment are shown by the solid symbols. These results were calculated using the aerodynamic angles of attack obtained by the method of Appendix B. The corresponding aerodynamic angles of attack are listed in the table on the figure. Point comparisons are not shown at supercritical Mach numbers since the tunnel interference analysis is not valid in this regime. The theoretical lift-coefficient variation with Mach number at a constant angle of attack is shown by the solid lines in Fig. 3. The constant angle of attack is the average of the aerodynamic angles of attack for M_∞=0.7 and 0.8. These limited comparisons show that fairly good agreement is achieved between theory and experiment.

The relative importance of the jet-sheet second order effect can be seen by comparing the dashed-line curve for K_π=1.0 with the solid line

[5]The angle of attack here is relative to a chord line through the leading and trailing edges of the mean camber line. The angle of attack (say $\breve{\alpha}$) employed in Refs. 8 and 9 is relative to an arbitrary chord line. The two angles of attack are related by $\alpha = \breve{\alpha} - 0.60$.

[6]The bulk of the data presented was for $\delta_j = 88°$, an unacceptably high value with which to make valid theoretical comparisons.

curve for the variable K_π shown. In this case the second order effect is significant. The dashed-dot line in Fig. 3 shows the incremental lift coefficient due to camber with blowing, $(\Delta c_\ell)_K$, where

$$(\Delta c_\ell)_K \equiv \frac{K}{\beta_\infty}\left[c_{\ell_K}(\beta_\infty K_\pi c_j) - c_{\ell_K}(0)\right] \tag{75}$$

Details regarding the calculation of c_{ℓ_K} are given in Appendix C. The incremental blown-camber-line contribution is frequently neglected for the reasons noted in Appendix C. For the example of Fig. 3, however, although $(\Delta c_\ell)_K$ is small, it is of sufficient magnitude to warrant its inclusion.

AIR FORCE/CONVAIR/CANADIAN TESTS

These tests (Refs. 10, 11, 12, and 13) were conducted in the Canadian National Aeronautical Establishment (NAE) two-dimensional, high-Reynolds number, transonic wind tunnel at Ottawa, Ontario. This tunnel has a 60x60-inch test section, porous upper and lower walls, and employs sidewall inserts to form a 15x60-inch, two-dimensional test section. Several different jet-flapped supercritical-type airfoils were tested in the series of tests reported in the cited references. The airfoil with which comparisons are made herein was designated as an NAE 001002 airfoil, possessed considerable aft camber, and had a chord of 15 inches. Forces and moments were measured by sidewall balances with supplementary data taken by a wake survey rake. A tunnel-interference angle-of-attack correction of the same form as Eq. 1 in Appendix B was applied. The factor k, however, was obtained from drag and axial momentum considerations rather than in the manner of Appendix B. Considerable spread in the value of k was found, but a single mean value of 0.55 per degree was employed in the data reduction.

A comparison of the results given by the subsonic similarity relation of Eq. 74 with some NAE test data is given in Fig. 4. Figure 4 shows that rather good agreement is obtained for subcritical Mach numbers. Note also that the lift-coefficient increment due to the blown camber line is significant.

Some comment is appropriate regarding the reference angle of attack, $\breve{\alpha}'$, employed in Fig. 4. When the unblown experimental data used for Fig. 4 was reduced to zero Mach number by the Prandtl-Glauert relation, the angle of zero lift was found to occur at a 0.66-degree angle higher than predicted by thin-airfoil theory. This discrepancy is assumed to be due to a constant geometric error in the experiments, which is equivalent to considering the angle of attack to be measured from a chord line different from that specified.[7] In the present case, the angles of attack (in degrees) relative to the specified and apparent chord lines are related by $\breve{\alpha}' = \breve{\alpha} - 0.66$.

The camber-line aerodynamics for Fig. 4 was calculated by the method of Appendix C for an arbitrary camber-line shape. Note also that the angles of attack (in degrees) relative to the specified chord line and the camber-line chord are related by $\breve{\alpha} = \alpha - 0.34$.

The relative importance of the jet-sheet second order effect can be seen by comparing the dashed-line curve for $K_\pi = 1.0$ with the solid-line curve for the variable K_π shown. In this case the second-order effect is negligible. For a jet-momentum coefficient of a magnitude sufficient to choke the jet nozzle at a free-stream Mach number less than 0.5, the second-order effect would be significant.

FRENCH O.N.E.R.A. TESTS

The French tests (Ref. 14) were conducted on a half-span rectangular wing model of aspect ratio 3.4. The airfoil section is an NACA 64A010 airfoil truncated and modified at the 88% chord position yielding a 11.4% thick airfoil. Further details on the model and facility were not available.

[7]This assumption is justified by an improved agreement between theory and experiment.

In applying the subsonic similarity law, Hartunian's theory (Ref. 15) for a finite-span jet-flapped wing is employed to obtain the wing characteristics at zero Mach number. On the basis of Hartunian's relations, the lift, induced angle of attack, and induced drag, respectively, are given by:

$$(C_L)_{M_\infty=0} = \frac{\alpha c_{\ell_\alpha}\ (c_j) + \delta_j\, c_{\ell_{\delta_j}}\ (c_j)}{1 + \dfrac{c_{\ell_{\delta_j}}\ (c_j)}{\pi A + 2c_j}} \tag{76}$$

$$(-\Theta_i)_{M_\infty=0} = \frac{(C_L)_{M_\infty=0}}{\pi A + 2c_j} \tag{77}$$

$$(C_{D_i})_{M_\infty=0} = (-\Theta_i)_{M_\infty=0}\ (C_L)_{M_\infty=0} = \frac{(C_L^{\,2})_{M_\infty=0}}{\pi A + 2c_j} \tag{78}$$

Taking $\varepsilon=\beta_\infty^{\,3}$, $\Omega=1$, $\sigma=\alpha$, and $\omega=-1$ in Eq. 69 yields the similarity relations

$$C_L = \frac{1}{\beta_\infty}\left[\frac{\alpha c_{\ell_\alpha}(\beta_\infty K_\pi c_j) + \delta_j\ c_{\ell_{\delta_j}}\ (\beta_\infty K_\pi c_j)}{1 + \dfrac{c_{\ell_{\delta_j}}\ (\beta_\infty K_\pi c_j)}{\pi\beta_\infty A + 2\beta_\infty K_\pi c_j}}\right] \tag{79}$$

$$(-\Theta_i) = (-\Theta_i)_{M_\infty=0} \qquad C_{D_i} = (-\Theta_i)_{M_\infty=0}\ C_L \tag{80}$$

Determination of K_π in Eq. 79 requires values for the relative nozzle height, h_j/c, and the nozzle-flow coefficient, c_n. Since neither of these quantities was available in the referenced document, guessed values were employed. For this purpose, the nozzle-flow coefficient was taken to be unity and h_j/c to be 0.008. The value of h_j/c was selected in the following manner. For tests conducted on an NACA 0018 airfoil in Ref. 14, the average value of h_j/c was 0.0129 (see Fig. 10 of Ref. 14). Ratioing this value according to wing thickness yields $h_j/c = 0.008$.

A comparison of the lift-coefficient scaling given by Eq. 79 with the experiments of Ref. 14 appears in Fig. 5, where reasonably good agreement is obtained for a jet-deflection angle of 29°, but poorer agreement is obtained for δ_j=-2°. Apparently the influence of K_π is negligible in this case.

SECTION V

CONCLUSIONS

Applying the known principles of scaling, linear-subsonic and nonlinear-transonic similarity rules have been derived for a finite-span-jet-flapped wing with partial or full-span blowing. In deriving the rules, an attempt was made to keep the presentation as general as possible in order to display the interrelation between the linear and nonlinear rules and to allow freedom in adjusting the scaling to emphasize the parameters and type of scaling most appropriate to a particular problem under consideration. Although this generalized approach makes the analysis slightly more difficult to follow, it is believed to be worthwhile for the additional visibility it provides.

The effect of jet-supply pressure ratio was delineated by considering second-order quantities in the jet-sheet compatibility condition. The importance of jet-supply pressure ratio depends upon the flight Mach number at which the jet nozzle (assuming a convergent configuration) chokes. At this time it is not known whether typical flight vehicles will fall within the parametric spectrum where jet-supply pressure ratio is an important consideration. In comparisons with three different sets of wind-tunnel data, jet-supply pressure ratio was found to be of significant importance for only one set of data considered.

This investigation also disclosed that camber-line effects with blowing assume more importance than heretofore was the case in jet-augmented mechanical flap applications.

Finally, although reasonably good agreement was obtained for limited comparisons with experiment for linear-subsonic flow, there is a critical need for well-designed wind-tunnel experiments to validate both the linear subsonic and nonlinear transonic similarity rules. The experiments should be planned to eliminate tunnel interference effects or should be conducted in a facility where the magnitude of the interference can be accurately predicted. In the tests parametric variations

should be made within ranges consistent with the small perturbation assumption of the similarity analysis. Parametric variations also should be specifically tailored to test three-dimensional effects and the nonlinear transonic rules.

APPENDIX A

SECOND-ORDER JET-SHEET COMPATIBILITY CONDITION FOR COMPRESSIBLE FLOW

For the jet sheet to be compatible with the external flow, the jet-sheet internal static pressures at the sheet upper and lower boundaries must be equal to the corresponding static pressures in the external flow, and the sheet boundaries must be stream surfaces of the external flow. In deriving the compatibility condition, the lateral-flow velocity perturbations are assumed to be negligible compared to the vertical and longitudinal ones, thereby permitting the jet-sheet flow to be treated as two-dimensional in any plane where y = a constant. A similar approach is employed by Maskell and Spence in their treatment (Ref. 16) of a finite-span jet-flapped wing. With reference to Fig. 2, it is also assumed that the jet-center-line radius of curvature, R, is large, the jet thickness, h, is very small, and the downward displacement of the jet is small, such that $h/R \ll 1$ and $R^{-1} \simeq - \partial\Theta_{js}/\partial x$.

In jet-flap applications the jet-exhaust-nozzle height, h_j, is usually rather small due to the geometrical constraints imposed by the thinness of the airfoil trailing edge. Consequently, for a convergent nozzle, choked (critical) flow may occur if the jet-supply pressure is sufficiently high. Assuming the jet-sheet internal flow is isentropic[1], the jet flow downstream of the nozzle will have a differing character for subcritical and supercritical nozzle flow conditions. For sub-critical nozzle flows the magnitude of the nozzle exit pressure will be essentially governed by the external freestream static pressure. For the limiting case of zero jet thickness in Spence's incompressible flow analysis (Ref. 17), it is implicit that the static pressure along the jet center line is equal to the freestream static pressure. As will be seen subsequently in this appendix, this condition is also approximately

[1] In the real flow, shock waves are likely to be present. The assumption of isentropy is an approximation, strictly valid for supercritical duct-supply pressures only slightly exceeding the critical presssure

true for a first-order compressible flow. If, however, the nozzle flow is supercritical, the nozzle static pressure is governed by the jet-supply pressure and may on the average be greater than the freestream static pressure. In the analytical modeling for this case, therefore, some provisions must be made for accounting for the longitudinal decay of the center-line over-pressure within the jet. This can be accomplished by a second (or higher) order analysis of the jet-sheet internal flow, as in this appendix.

With reference to Fig. 2, the internal and external-flow field horizontal-velocity components are given respectively by

$$\hat{u} = \hat{U}_\infty + \hat{u}' \qquad u = U_\infty + u' \qquad \text{(A-1), (A-2)}$$

where $\hat{u}' << \hat{U}_\infty$ and $u' << U_\infty$.

The irrotationality condition, in natural coordinates (n,s), is given by Ref. 6 as

$$\frac{1}{\hat{u}} \frac{\partial \hat{u}}{\partial n} = \frac{1}{r} \qquad \text{(A-3)}$$

Expanding r along n gives

$$r \simeq R + (\partial r/\partial n)_o n + \text{-----} \qquad \text{(A-4)}$$

Substituting Eq. A-4 in Eq. A-3, integrating, and applying the condition $\hat{u}=\hat{u}_o$ at n=0, yields

$$\frac{\hat{u}}{\hat{u}_o} = \exp\left[\frac{n}{R} - \frac{1}{2}\left(\frac{\partial r}{\partial n}\right)_o \frac{n^2}{R^2} + \text{---}\right] \qquad \text{(A-5)}$$

Assuming $[1-(\partial r/\partial n)_o] << 1$ and $(n/R) << 1$, making use of Eq. A-1, and expanding Eq. A-5 yields to second order in small quantities

$$\hat{u}' = \hat{u}'_o + (\hat{U}_\infty + \hat{u}'_o)\,(n/R) \qquad \text{(A-6)}$$

To an order consistent with nonlinear transonic-flow theory, the pressure in the external stream is given by

$$p = p_\infty - \rho_\infty U_\infty^2 \, (u'/U_\infty) \tag{A-7}$$

The jet-sheet internal pressure to second order is

$$\hat{p} = \hat{p}_\infty - \hat{\rho}_\infty \hat{U}_\infty^2 \left[\frac{\hat{u}'}{\hat{U}_\infty} + \frac{1}{2} \, (1-\hat{M}_\infty^2) \, \frac{\hat{u}'^2}{\hat{U}_\infty^2} \right] \tag{A-8}$$

Along the center line, Eq. A-8 gives

$$\hat{p}_o = \hat{p}_\infty - \hat{\rho}_\infty \hat{U}_\infty^2 \left[\frac{\hat{u}'_o}{\hat{U}_\infty} + \frac{1}{2} \, (1-\hat{M}_\infty^2) \, \frac{\hat{u}'^2_o}{\hat{U}_\infty^2} \right] \tag{A-9}$$

The internal pressures at the upper and lower jet boundaries are given by substituting $\hat{u}'_u$ and $\hat{u}'_\ell$ respectively in Eq. A-8, where from Eq. A-6, $\hat{u}'_u$ and $\hat{u}'_\ell$ are given respectively by

$$\hat{u}'_u = \hat{u}'_o + \frac{1}{2} \, (\hat{U}_\infty + \hat{u}'_o)(h/R) \tag{A-10}$$

$$\hat{u}'_\ell = \hat{u}'_o - \frac{1}{2} \, (\hat{U}_\infty + \hat{u}'_o)(h/R) \tag{A-11}$$

Applying the boundary conditions

$$\hat{p}_u = p_u \text{ and } \hat{p}_\ell = p_\ell \tag{A-12}$$

and employing Eqs. A-8, A-10 and A-11 yields to second order, the result

$$p_u - p_\ell = - \hat{\rho}_\infty \hat{U}_\infty^2 \, (\frac{h}{R}) \left[1 + (2-\hat{M}_\infty^2) \, (\frac{\hat{u}'_o}{\hat{U}_\infty}) \right] \tag{A-13}$$

The variable h(s) may be determined from global continuity. Application of continuity between downstream infinity and an arbitrary s-station yields

$$h_\infty = \int_{-h/2}^{h/2} (\hat{\rho}/\rho_\infty)(\hat{u}/\hat{U}_\infty) \, dn \tag{A-14}$$

Employing Eq. 39 of Ref. 4, the density to second order is

$$\frac{\hat{\rho}}{\hat{\rho}_\infty} = 1-\hat{M}_\infty^2 \left\{ \frac{\hat{u}'}{\hat{U}_\infty} + \frac{1}{2} \left[1-(2-\gamma)\hat{M}_\infty^2\right] \frac{\hat{u}'^2}{\hat{U}_\infty^2} \right\} \tag{A-15}$$

Making use of Eqs. A-2, A-6, and A-15 in Eq. A-14 yields, to second order

$$\frac{h}{R} = \left[1 - (1-\hat{M}_\infty^2) \frac{\hat{u}_o'}{\hat{U}_\infty}\right] \frac{h_\infty}{R} \tag{A-16}$$

Substituting Eq. A-16 in Eq. A-13 yields, to second order

$$p_u - p_\ell = -(\hat{\rho}_\infty \hat{U}_\infty h_\infty) \left(1+ \frac{\hat{u}_o'}{\hat{U}_\infty}\right) \frac{\hat{U}_\infty}{R} \tag{A-17}$$

Solving Eq. A-9 for $(\hat{u}_o'/\hat{U}_\infty)$ *and substituting the result in Eq. A-17 yields, to second order*

$$p_\ell - p_u = - C_\pi \left(\hat{\rho}_\infty \hat{U}_\infty h_\infty\right) \hat{U}_\infty \left(\frac{\partial \Theta_{js}}{\partial x}\right) \tag{A-18}$$

where

$$C_\pi \equiv 1 - \frac{\hat{p}_o - p_\infty}{\gamma \hat{p}_\infty \hat{M}_\infty^2} \tag{A-19}$$

and R has been replaced by the approximation $R^{-1} \simeq -\partial\Theta_{js}/\partial x$. The parameter C_π, which varies longitudinally, is a factor modifying the usual jet-sheet compatibility condition.

It is of interest to examine C_π in more detail.

If, from Eqs. A-8, A-10, and A-11, an expression for $(\hat{p}_u + \hat{p}_\ell)$ is derived, and in this expression Eqs. A-9, A-16, and A-12 are substituted respectively for $(\hat{u}_o/\hat{U}_\infty)$, (h/R), $\hat{p}_u$, and $\hat{p}_\ell$, the following result is obtained to second order

$$\hat{p}_o = \frac{p_u + p_\ell}{2} + \frac{\hat{\rho}_\infty \hat{U}_\infty^2}{8} (1-\hat{M}_\infty^2) \left(\frac{h_\infty}{R}\right)^2 \tag{A-20}$$

In the vicinity of the jet sheet, let

$$u' = u'_s + u'_{as} \tag{A-21}$$

where u'_s and u'_{as} are respectively the symmetrical and antisymmetrical parts of the perturbation velocities relative to the jet center such that

$$u'_{s_u} = u'_{s_\ell} \equiv u'_s; \quad (u'_{as})_u = -(u'_{as})_\ell \tag{A-22), (A-23}$$

From Eqs. A-7, A-22, and A-23, it is easily shown that

$$(1/2)(p_u + p_\ell) = p_\infty - \rho_\infty U_\infty^2 (u'_s/U_\infty) \tag{A-24}$$

Recalling that $\hat{p}_\infty = p_\infty$, Eqs. A-20 and A-24 yield, to first order

$$\frac{\hat{p}_o - p_\infty}{\gamma \hat{p}_\infty \hat{M}_\infty^2} = -\left(\frac{M_\infty^2}{\hat{M}_\infty^2}\right)\left(\frac{u'_s}{U_\infty}\right) \tag{A-25}$$

The velocity u'_s is a free-stream perturbation velocity at the jet boundaries due to jet thickness. The important point here is that to first order $\hat{p}_o(s)$ is equivalent to the pressure distribution along the center line of a thin jet of finite thickness exhausting at zero inclination into a surrounding stream. Consequently, $\hat{p}_o(x)$ can be determined independently of the more general curved jet-sheet flow problem.

For subcritical nozzle flow into a subsonic external stream it is well known that $\hat{p}_j = p_\infty$ and hence it is reasonable to take $\hat{p}_o(x) = p_\infty$ for this case. For choked nozzle flow into an incompressible external stream, an approxiate solution for $\hat{p}_o(x)$ could possibly be found. With $\hat{p}_o(x)$ then known, Spence's (Ref. 17) integral equations could be appropriately modified and possibly solved. The resulting solutions could be extended to subsonic linear compressible flow by means of the similarity relations herein. The solutions so obtained would be functions of the supply duct pressure ratio $(\hat{P}/p_\infty)$ in addition to c_j. Note, however, that the present analysis is a small perturbation one, for which $(\hat{p}_o - p_\infty)/\gamma \hat{p}_\infty \hat{M}_\infty^2 \ll 1.0$, from which it follows that $C_\pi \to 1.0$.

With this in mind, it hardly seems worthwhile to treat C_π as a variable. Instead, a constant average value $\langle C_\pi \rangle$ will be sought such that

$$\langle C_\pi \rangle = 1.0 \qquad \text{for} \qquad \hat{P}/p_\infty \leq \hat{P}/\hat{p}_* \tag{A-26}$$

$$\langle C_\pi \rangle \neq 1.0 \qquad \text{for} \qquad \hat{P}/p_\infty \geq \hat{P}/\hat{p}_* \tag{A-27}$$

where

$$(\hat{P}/\hat{p}_*) = (1/2 + \gamma/2)^{\gamma/\gamma-1} = 1.893 \ (\gamma = 1.4) \tag{A-28}$$

To determine $\langle C_\pi \rangle$ for the choked-nozzle-flow case, assume that

$$\langle \hat{p}_o \rangle = 1/2 \ (\hat{p}_j + \hat{p}_\infty) \equiv 1/2 \ (\hat{p}_* + p_\infty) \tag{A-29}$$

This yields

$$\langle C_\pi \rangle \equiv 1 - \frac{(\hat{p}_*/p_\infty) - 1}{2\gamma \hat{M}_\infty^{\ 2}} \tag{A-30}$$

For subcritical nozzle flow, the flow field across the nozzle is affected by the external stream, generally is nonuniform, and therefore is inappropriate for use as a reference stream. In the previous analyses, this is one reason for referencing the local-flow state within the jet sheet to the jet internal flow at downstream infinity. For choked or supersonic nozzle flow, the details of the flow across the nozzle are governed by the upstream conditions in the nozzle duct, and the duct contours can be designed to give a uniform flow at the nozzle exit. Hence, from the standpoint of flow uniformity the nozzle exit flow can be used as a reference stream. However, for this case, when the nozzle flow is sonic, the assumption of small perturbations is locally invalid. This, then, is a second reason for employing the downstream jet flow as a reference stream in the previous perturbation analyses. Tentatively, disregarding the second reason, a perturbation analysis from a choked nozzle stream can be employed to yield additional insight regarding $\langle C_\pi \rangle$.

A perturbation analysis paralleling that performed for $\hat{M}_\infty$ will now be outlined for flow perturbations referenced to the nozzle exit.

For convenience in discussion, the nozzle-exit Mach number is tentatively assumed to be arbitrary. For the aforementioned analysis, the applicable equations are of the same form as the Eqs. A-1 through A-19, with the flow-state variables at downstream infinity within the jet sheet replaced by those at the jet-nozzle exit. With these considerations in mind, evoking continuity within the jet, and taking the jet exit Mach number to be unity, the following result may be deduced by analogy with Eqs. A-18 and A-19.

$$p_\ell - p_u = -(\hat{\rho}_\infty \hat{U}_\infty h_\infty)\hat{U}_\infty \left(\frac{\hat{a}_*}{\hat{U}_\infty}\right)\left(1+\frac{\hat{p}_*-\hat{p}_\infty}{\gamma \hat{p}_*}\right)\left(\frac{\partial \Theta_{js}}{\partial X}\right) \tag{A-31}$$

Making use of Eq. 38 in Ref. 4, it may be shown that to first order

$$\left(\frac{\hat{a}_*}{\hat{U}_\infty}\right) = 1 - \frac{\hat{p}_*-\hat{p}_\infty}{\gamma \hat{p}_*} \tag{A-32}$$

for $(\hat{p}_*-\hat{p}_\infty)/\gamma\hat{p}_* << 1.0$ substituting Eq. A-32 in Eq. A-31 yields to second order the result

$$p_\ell - p_u = -C'_\pi (\hat{\rho}_\infty \hat{U}_\infty h_\infty)\hat{U}_\infty \left(\frac{\partial \Theta_{js}}{\partial x}\right) \tag{A-33}$$

where

$$C'_\pi \equiv \left(1 - \frac{\hat{p}_o - p_\infty}{\gamma p_*}\right) \tag{A-34}$$

If, as before, a mean value of p_o given by Eq. A-29 is employed, the mean value of C'_π is

$$\langle C'_\pi \rangle \equiv 1 - \frac{\hat{p}_* - p_\infty}{2\gamma \hat{p}_*} \tag{A-35}$$

For

$$\hat{P}/\hat{p}_* \leq (\hat{P}/p_\infty) \leq 5 \tag{A-36}$$

it is found that

$$\langle C_\pi \rangle \simeq \langle C'_\pi \rangle \tag{A-37}$$

where $\langle C_\pi \rangle$ and $C'_\pi \rangle$ differ from each other by less than 3%. In view of its simpler form, $\langle C'_\pi \rangle$ will be employed. The second order jet-sheet compatibility condition then becomes

$$C_{p_\ell} - C_{p_u} = -K_\pi c_j c \left(\frac{\partial \Theta_{js}}{\partial x}\right) \tag{A-38}$$

where

$$\begin{aligned} K_\pi &= 1.0 && \text{for} && (\hat{P}/p_\infty \leq \hat{P}/\hat{p}_*) \\ K_\pi &= 1 - \frac{1}{2\gamma}\left(1 - \frac{\hat{P}/\hat{p}_*}{\hat{P}/p_\infty}\right) && \text{for} && ((\hat{P}/\hat{p}_*) \leq (\hat{P}/p_\infty) \leq 5 \end{aligned} \tag{A-39}$$

APPENDIX B

INTERFERENCE CORRECTION FOR AIR FORCE/NORTHROP TESTS

The small magnitude of the lift-curve slopes for the unblown-airfoil data in Refs. 8 and 9 at the sub-critical Mach numbers of 0.7 and 0.8 indicates that interference effects were likely present in the tests. Although there is no independent data available to directly support this contention, an engineering estimate can be made by transforming the slopes to the incompressible-flow regime ($M_\infty \simeq 0$) by the Prandtl-Glauert rule[1] and comparing these with a variety of data for approximately similar airfoils.

Application of the Prandtl-Glauert rule to the unblown airfoil data of Figs. A-1 and A-2 in Ref. 9 yields incompressible-flow lift-curve slopes of 3.7 and 3.5 per radian respectively. For six percent thick airfoils of the NACA 6-series type, the low Mach number experimental lift-curve slopes documented in Ref. 19 for eight different airfoils are 6.42, 6.30, 6.25, 6.25, 6.02, 6.02, 5.73, and 6.19 per radian. The foregoing comparisons support the contention that the data of Refs. 8 and 9 are in error due to interference effects.

The average lift-curve slope for the eight airfoils cited above is 6.15 per radian. For convenience and in view of the uncertainties involved, however, the theoretical value of 2π will be employed in the analysis which follows.

The interference-induced angle of attack (geometrical angle of attack, α_g, minus the actual aerodynamic angle of attack, α) in the wind tunnel is assumed to be given by

$$\alpha_g - \alpha = c\ell_\Gamma / k \qquad \text{(B-1)}$$

[1] It is generally conceded (see, e.g., Ref. 18) that the Prandtl-Glauert correction to the lift-curve slope gives reasonably good results for subcritical Mach numbers.

where k is the interference factor which is to be determined. A similar correction is applied to the data of Refs. 10 through 13, except that k is determined in a different manner. Differentiating and manipulating Eq. B-1 yields

$$k = \frac{dc_{\ell_\Gamma}/d\alpha_g}{1 - \frac{dc_{\ell_\Gamma}/d\alpha_g}{dc_{\ell_\Gamma}/d\alpha}} \tag{B-2}$$

where $dc_{\ell_\Gamma}/d\alpha_g$ is the lift curve slope in the wind tunnel and $dc_{\ell_\Gamma}/d\alpha$ is the true lift curve slope in free air. Equation B-2 applies to both the unblown and blown airfoils, since c_{ℓ_Γ} is the circulation lift coefficient. However, the unblown airfoil data only is used to obtain k values which are then applied to the blown airfoil in correlating the similarity rules with experiment. The lift-curve slope required in Eq. B-2 is obtained from

$$\left(\frac{dc_{\ell_\Gamma}}{d\alpha}\right)_{M_\infty} = \beta_\infty^{-1}\left(\frac{\partial c_{\ell_\Gamma}}{\partial \alpha}\right)_{M_\infty=0} \tag{B-3}$$

where, as previously stated, the incompressible-flow slope is taken to be 2π.

From the unblown airfoil data of Figs. A-1 and A-2 in Ref. 9, k was determined to be 12.38 and 13.41 per radian respectively for free-stream Mach numbers of 0.7 and 0.8.

APPENDIX C

ANALYSIS OF CAMBERED JET-FLAPPED AIRFOILS

The most common application of the jet-flap principle to date has been to jet-augmented mechanical flaps for use during the take-off and landing flight phases. For this application, the lift coefficients achieved are very high and the relative lift contribution due to camber-line jet-sheet interaction is negligible. For pure jet-flapped wings at high speeds, the camber-line contribution, although small, can be a relatively higher fraction of the total lift and should be taken into account in some instances. Because of previous emphasis on very high-lift applications, little attention has been given to the analysis of camber-line effects. The sole investigation on the subject appears to be that of Hough (Ref. 20), who has formulated an analysis for a polynomial camber line, but has provided specific numerical results only for the parabolic case. There is a need for a prediction capability for arbitrary camber-line shapes, since the parabolic camber line is not necessarily the best one for high-speed applications. Supercritical airfoils, for example, are possible candidates for jet-flap application. Many of these, such as the NAE 001002 airfoil treated herein, are typified by considerable aft camber.

Before pursuing the subject of arbitrary camber further, it is of interest to comment on Hough's parabolic results. Hough notes that, as a consequence of his employment of a 3-control-point calculation procedure, his results may be in error at low values of the momentum coefficient. Since at high speeds the momentum coefficient is typically small and since one of the airfoils examined in this report has an approximately parabolic camber line, it was deemed of interest to investigate the magnitude of the error noted by Hough. Consequently, the derivatives $\partial c_\ell/\partial\kappa$ and $\partial c_m/\partial\kappa$ were recalculated using a 9-control-point calculation. The resulting curves, along with a 3-point calculation, are plotted on Fig. 6. Figure 6 shows that the error for the 3-control-point calculation increases significantly as the momentum coefficient approaches zero.

One could further develop the Hough formulation for polynomial camber lines for possible application to arbitrary camber lines. It appears, however, that the development would tend to become unwieldly for higher-degree polynomials, and even these might not adequately represent some camber lines. Instead, an alternative method is presented herein. The calculation procedure for this method involves only a simple quadrature, is easily understood, and is readily performed by hand.

Applying the principle of superposition, the solution for a jet-augmented, single-element, mechanical-flapped airfoil given in Ref. 21 can be used to obtain a solution for the segmented airfoil shown in Fig. 7. The segmented airfoil, in turn, can be considered to be an approximation to a continuous camber line. On this basis, the lift coefficient and leading-edge pitching moment coefficient due to camber for the segmented airfoil of Fig. 7 with $\delta_j \approx 0$ are given respectively[1] by

$$(c_\ell)_\kappa = - \sum_{n=0}^{N} c_{\ell_\delta} (c_j, x_n) (\theta_n - \theta_{n-1}) \qquad \text{(C-1)}$$

$$(c_m)_\kappa = - \sum_{n=0}^{N} c_{m_\delta} (c_j, x_n) (\theta_n - \theta_{n-1}) \qquad \text{(C-2)}$$

$$\text{where } \theta_n = \frac{y_{n+1} - y_n}{x_{n+1} - x_n} \qquad \text{(C-3)}$$

$$\text{and } x_0 = 0 \text{ and } \theta_{-1} = \theta_N = 0 \qquad \text{(C-4)}$$

[1] A method which avoids the use of camber-line slopes and is more accurate than Eqs. C-1 and C-2 can be obtained by formulating the integrals resulting from taking the limiting process in Eqs. C-1 and C-2. These integrals can be integrated twice by parts yielding integrals whose integrands involve the camber-line ordinate multiplied by an influence function. The influence functions required in this approach were not available at the time of this investigation, hence Eqs. C-1 and C-2 are employed in the present calculations as a matter of expediency. The details and influence functions for this second method will be published in a technical paper at a later date.

The derivatives c_{ℓ_δ} and c_{m_δ} are given in Ref. 21[2]. In applying Eqs. C-1 through C-4, the spacings employed can be adjusted locally according to whether Θ is varying rapidly or slowly.

A comparison of the results, using Eq. C-1, with a 9-control-point calculation for a parabolic camber line is shown in Fig. 6. For the calculation shown in this figure, the segmented mean line consisted of straight lines drawn between x stations of 0, 0.05, 0.1, 0.2, 0.3, 0.4, 0.5, 0.6, 0.7, 0.8, 0.9, 0.95 and 1.00 on the actual mean line. As can be seen, the agreement with the more exact calculation is excellent.

In general, for the incompressible flow about a pure jet-flapped thin airfoil, the lift and moment coefficients are given respectively by

$$c_\ell = \frac{\partial c_\ell}{\partial \kappa} \kappa + \frac{\partial c_\ell}{\partial \alpha} \alpha + \frac{\partial c_\ell}{\partial \delta} \delta_j \qquad \text{(C-5)}$$

$$c_m = \frac{\partial c_m}{\partial \kappa} \kappa + \frac{\partial c_m}{\partial \alpha} \alpha + \frac{\partial c_m}{\partial \delta_j} \delta_j \qquad \text{(C-6)}$$

where the derivatives with respect to α and δ_j are given in Ref. 21 and the derivatives with respect to κ for a parabolic camber line are given in Fig. 6.

[2]Additional values were calculated at x= .1, .2, .3, .4, by a non-linear interpolation method assuming the variation with x_n to be similar to the c_j=0 case.

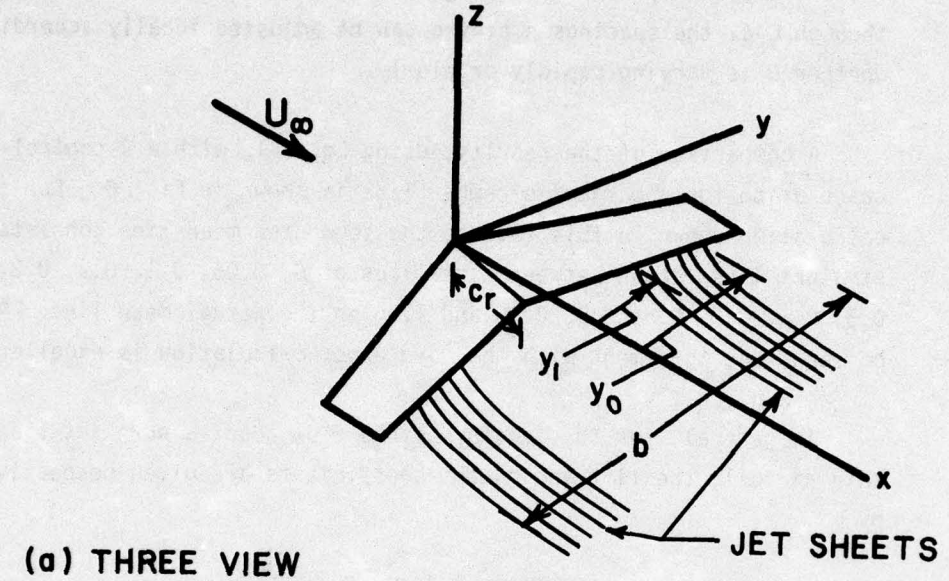

(a) THREE VIEW

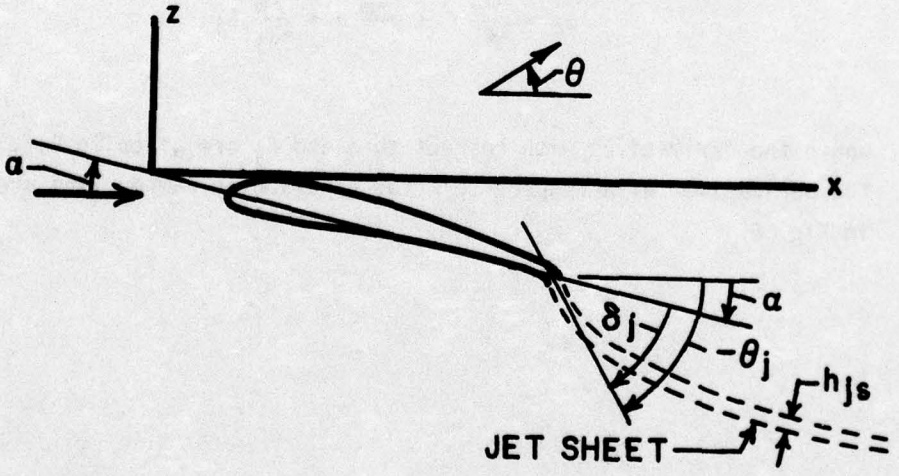

(b) SIDE VIEW (ARBITRARY y)

Figure 1. Illustration of Flow Problem and Notation

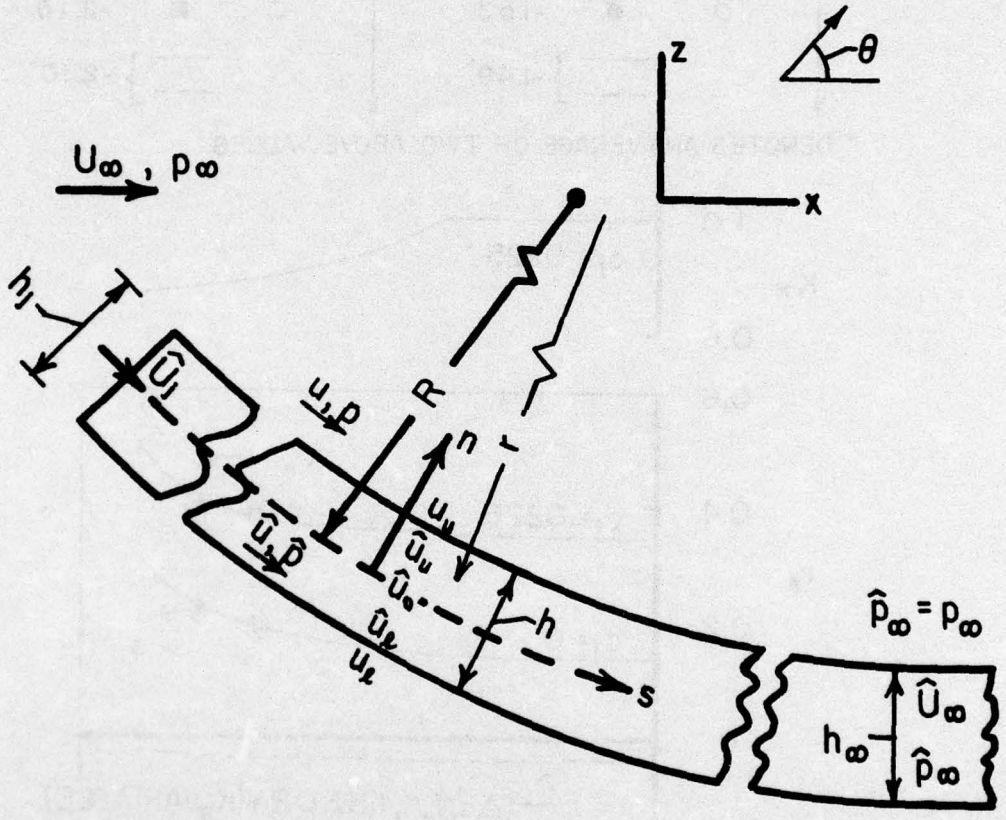

Figure 2. Notation for the Jet Sheet

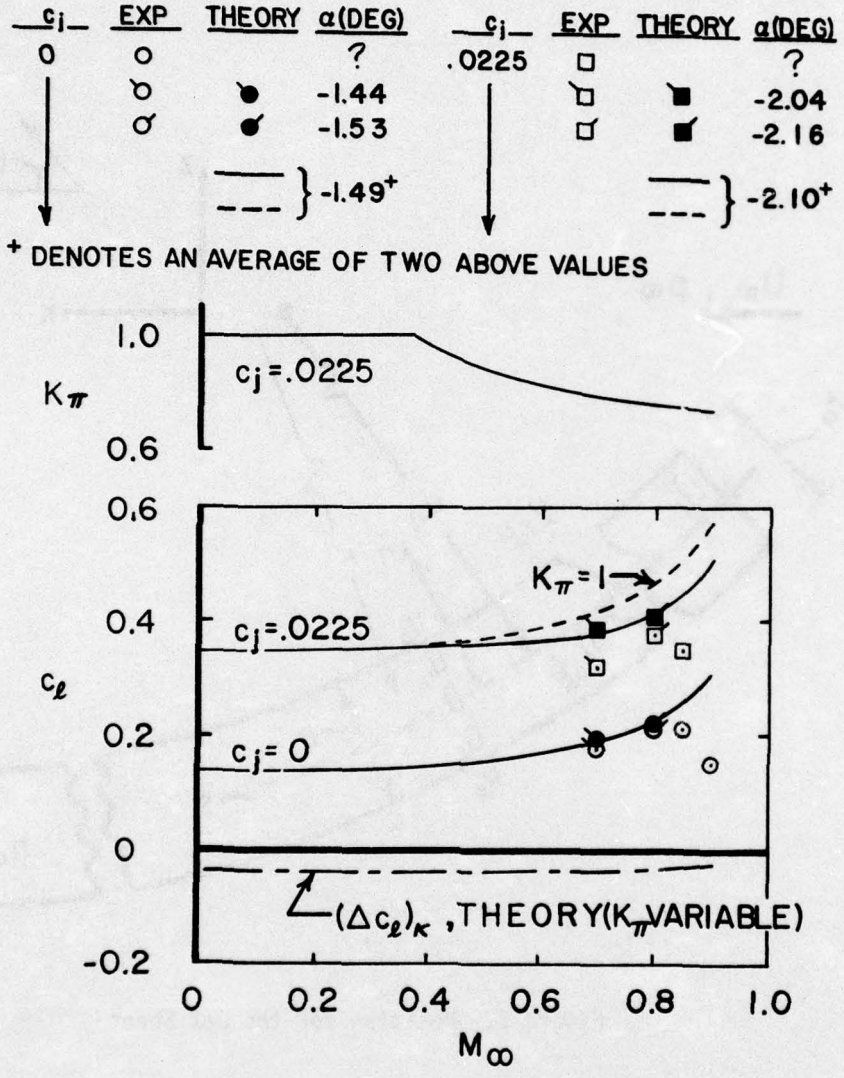

Figure 3. Comparison of Theory and Experiment for Air Force/Northrop Tests on a Modified NACA 64A406 Airfoil Section (Refs. 8 and 9); α_g=-0.63 Deg, δ_j = 35 Deg, h_j/c=0.0020

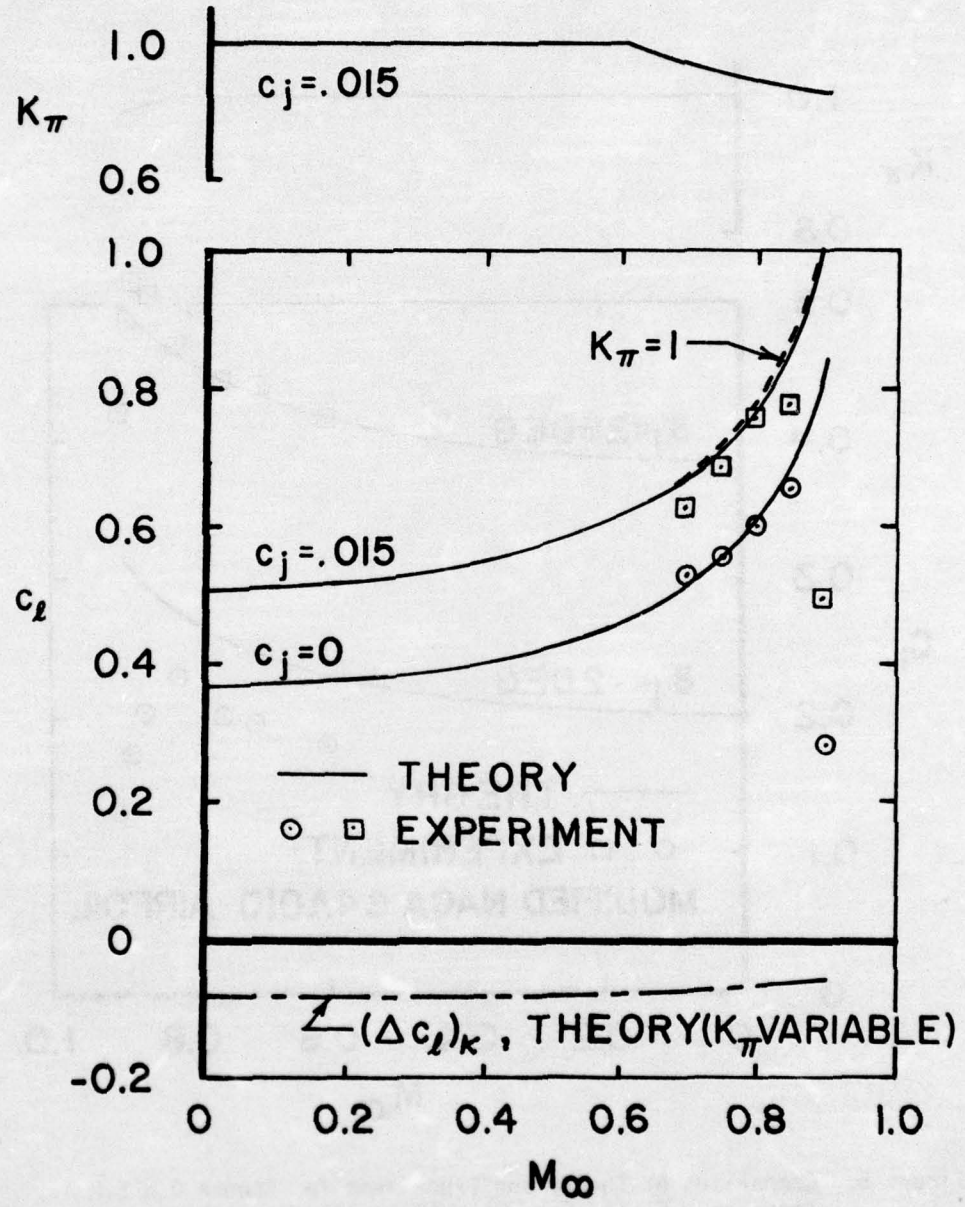

Figure 4. Comparison of Theory and Experiment for Air Force/Convair/ Canadian Tests on an NAE 001002 Airfoil Section (Refs. 10, 11, 12, and 13); $\breve{\alpha}'$ = -0.66 Deg, δ_j = 30 Deg, h_j/c=0.0030

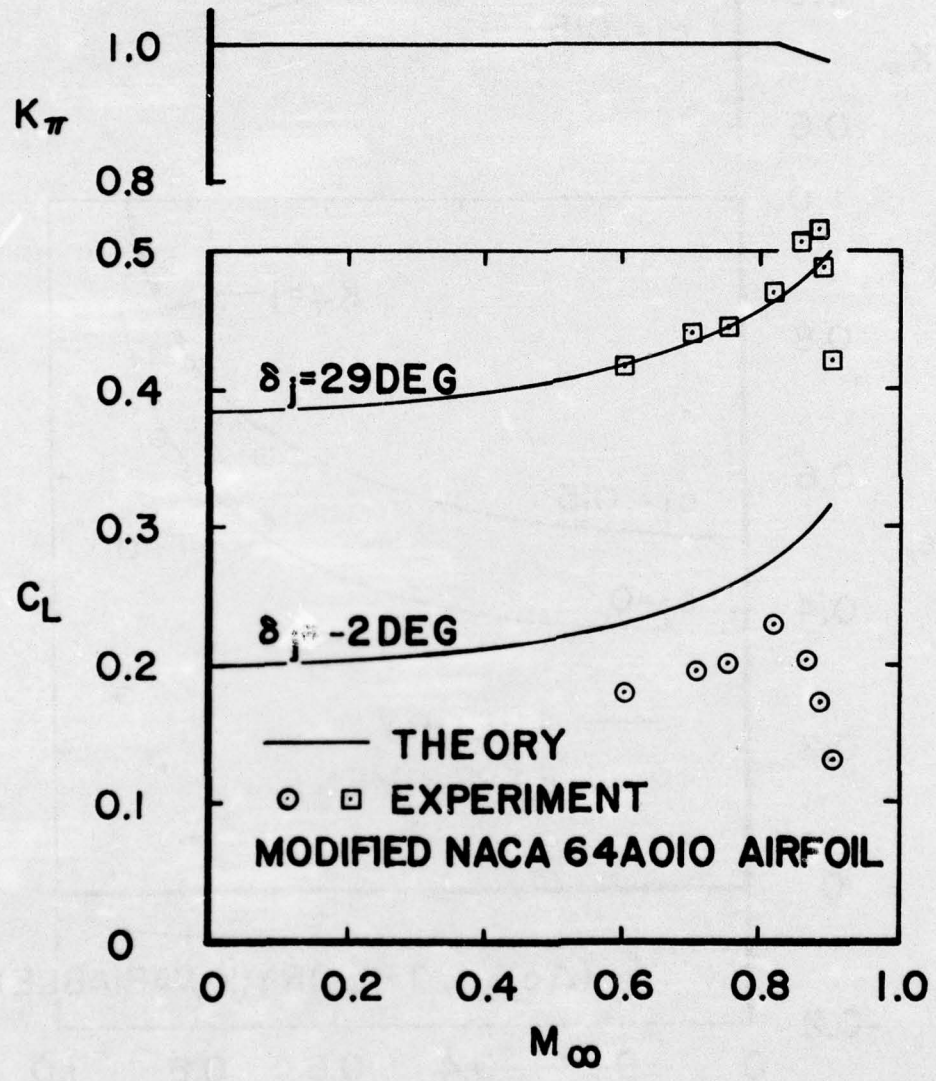

Figure 5. Comparison of Theory and Experiment for French O.N.E.R.A., Tests on a Finite-Span Wing (Ref. 14); α = 3 Deg, c_j = 0.023, A = 3.4, h_j/c = 0.0080 (Guess)

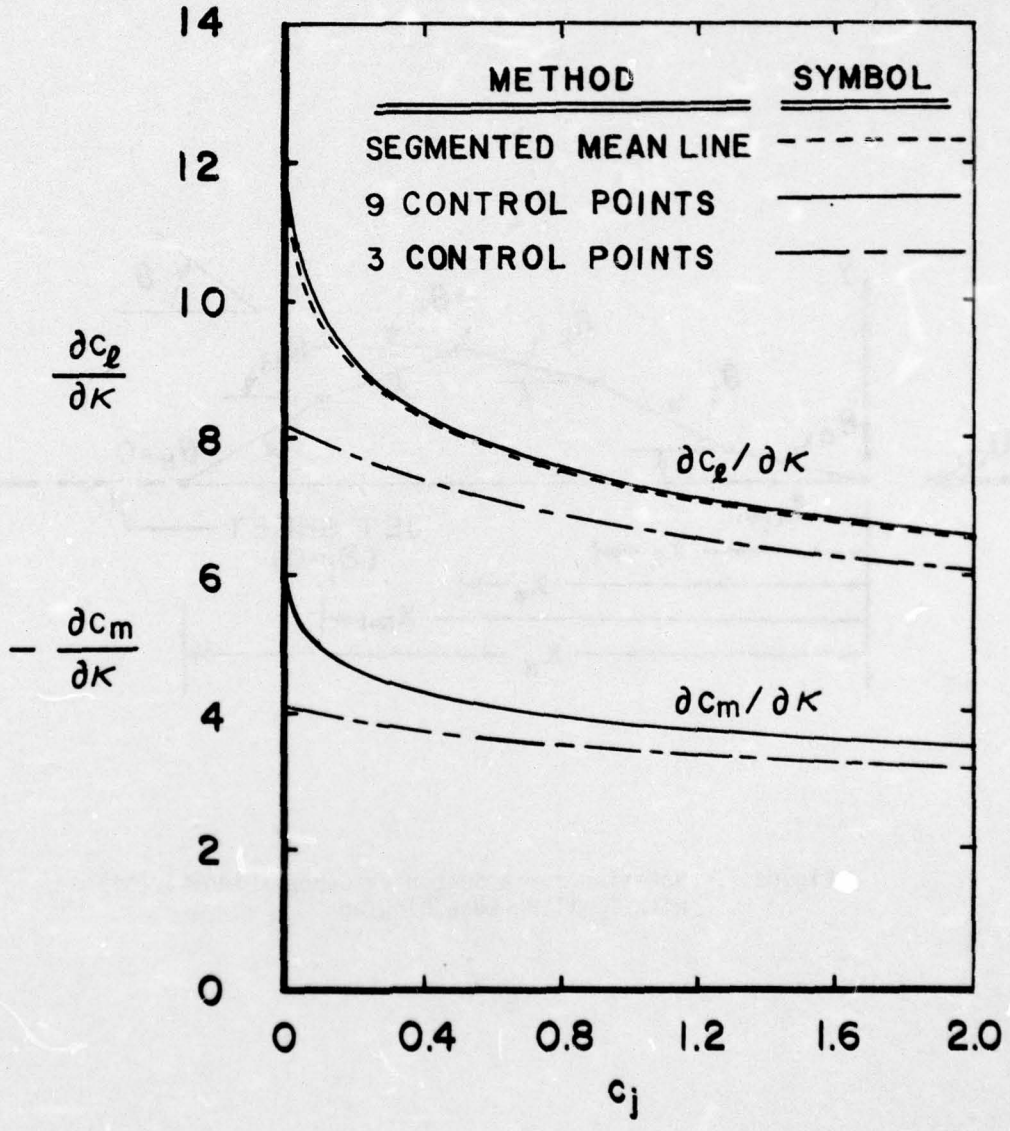

Figure 6. Comparison of Three Different Calculative Procedures for a Parabolically Cambered Jet-Flapped Airfoil

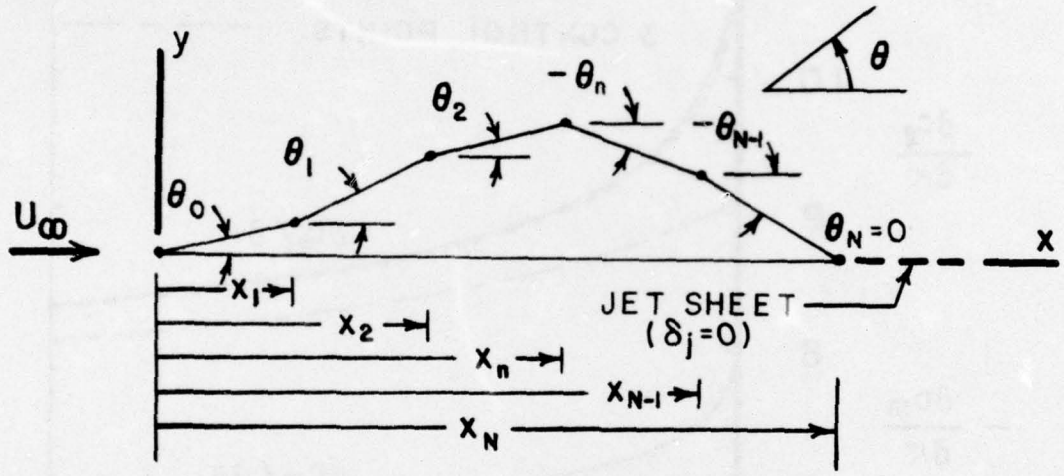

Figure 7. Notation for a Segmented-Camber-Line Airfoil with Trailing-Edge Blowing

REFERENCES

1. Siestrunk, R.: General Theory of the Jet Flap in Two-Dimensional Flow. In Boundary Layer and Flow Control, Vol. 1, edited by G. V. Lachmann. Pergamon Press, 1961, p 359.

2. Levinsky, E. S.: Prandtl-Glauert Rule for Wings with Jet Flaps. General Dynamics/Convair Aerospace Division, Aerodynamics Technical Note TN-73-AE-11, June 1973.

3. Elzweig, S.: Subsonic Similarity Rule for Jet-Flapped Airfoil. Journal of Aircraft, Vol. 8, No. 9, Sept. 1971, pp 744-5.

4. Ames Research Staff: Equations, Tables, and Charts for Compressible Flow, NACA Report 1135, 1953.

5. Spreiter, J. R.: On the Application of Transonic Similarity Rules to Wings of Finite Span. NACA Report 1153, 1953.

6. Liepmann, H. W. and Roshko, A.: Elements of Gasdynamics, John Wiley, 1957, pp 193, 255-263.

7. Krupp, J. A.: The Numerical Calculation of Plane Steady Transonic Flows Past Thin Lifting Airfoils. Boeing Scientific Laboratories Report D180-12958-1, June 1971 (N71-34275).

8. Grahame, W. E. and Headley, J. W.: Jet Flap Investigation at Transonic Speeds. Air Force Systems Command, AFFDL-TR-69-117, Feb. 1970.

9. Grahame, W. E., Headley, J. W. and Rogers, L. W.: Recent Experience in the Transonic Testing of Two-Dimensional Swept and Straight Wings with High Lift Devices. Paper No. 6 in AGARD Conference Proceedings No. 83, Facilities and Techniques for Aerodynamic Testing at Transonic Speeds and High Reynolds Number, AGARD CP-83-71, Aug. 1971 (N72-11854).

10. Yoshihara, H., Zonars, D. and Carter, W.: High Reynolds Number Transonic Performance of Advanced Planar Airfoils with Jet Flaps. Air Force Systems Command, AFFDL-TR-71-61, June 1971.

11. Peake, D. J., Yoshihara, H., Zonars, D. and Carter, W.: The Transonic Performance of Two-Dimensional, Jet-Flapped Aerofoils at High Reynolds Numbers. Paper No. 7 in AGARD Conference Proceedings No. 83, Facilities and Techniques for Aerodynamic Testing at Transonic Speeds and High Reynolds Number, AGARD CP-83-71, Aug. 1971 (N72-11854).

12. Peake, D. J. and Bowker, A. J.: Phase 1 Transonic Wind Tunnel Tests in the 15x60-Inch 2-D Insert Peakynosed, Aft-Cambered Airfoil Sections Incorporating Jet Flaps. National Research Council of Canada, NAE Report 5x5/0055, October 1972.

REFERENCES (Contd)

13. Bowker, A. J. and Peake, D. J.: Phase 2 Transonic Wind Tunnel Tests in the 15x60-Inch 2-D Insert of Peakynosed, Aft-Cambered Aerofoil Sections Incorporating Jet Flaps. National Research Council of Canada, NAE Report 5x5/0056, March 1973.

14. Malavard, L., Poisson-Quinton, Ph, and Jousserandot, P.: Jet-Induced Circulation Control, Part II-Experimental Results, Aero Digest, Vol. 73, No. 4. Oct. 1956, pp 46-59.

15. Hartunian, R. A.: The Finite Aspect Ratio Jet Flap. Cornell Aero Lab. Report Al-1190-A-3, October 1959.

16. Maskell, L. C. and Spence, D. A.: A Theory of the Jet Flap in Three Dimensions. Proceedings of Royal Society of London, Series A, Vol. 251, 1959.

17. Spence, D. A.: The Lift Coefficient of a Thin Jet-Flapped Wing. Proceedings of the Royal Society of London, Series A, Vol. 238, No. 1212, Dec. 1956.

18. Abbott, Ira H. and von Doenhoff, Albert E.: Theory of Wing Sections, Dover, 1959.

19. Hoak, D. E., Finck, R. D. et al: USAF Stability and Control DATCOM. Flight Control Division, Air Force Flight Dynamics Laboratory, Jan 1975.

20. Hough, G. R.: Cambered Jet-Flapped Airfoil Theory. Master of Aeronautical Engineering Thesis, Graduate School of Aeronautical Engineering, Cornell University, Ithaca, New York, Sept. 1959.

21. Spence, D. A.: The Lift on a Thin Aerofoil with a Jet-Augmented Flap. The Aeronautical Quarterly, Vol. IX, Aug. 1958, pp 287-299.

☆ U. S. GOVERNMENT PRINTING OFFICE: 1976 — 757-001/111